Bisphenol A Adsorption from Aqueous Solution using Graphene Oxide-Alginate Beads

Nurul Syazana Fuzil
Universiti Teknologi MARA
NUR HIDAYATI OTHMAN (nurhidayati0955@uitm.edu.my)
Universiti Teknologi MARA https://orcid.org/0000-0002-8396-2947
Nur Ain Shazwani Roslee Ab. Jamal
Universiti Teknologi MARA
ANA NAJWA Mustapa
Universiti Teknologi MARA
NUR HASHIMAH ALIAS
Universiti Teknologi MARA
'AQILAH DOLLAH
Universiti Teknologi MARA
Nik Raikhan NIK HIM
UiTM: Universiti Teknologi MARA
FAUZIAH MARPANI
UiTM: Universiti Teknologi MARA

Research Article

Keywords: alginate, graphene oxide, BPA, adsorption, wastewater treatment

Posted Date: February 23rd, 2021

DOI: https://doi.org/10.21203/rs.3.rs-221643/v1

Version of Record: A version of this preprint was published at Journal of Polymers and the Environment on July 2nd, 2021. See the published version at https://doi.org/10.1007/s10924-021-02226-y.

Bisphenol A Adsorption from Aqueous Solution using Graphene Oxide-Alginate Beads

Nurul Syazana Fuzil, Nur Hidayati Othman*, Nur Ain Shazwani Roslee Ab. Jamal, Ana Najwa Mustapa, Nur Hashimah Alias, 'Aqilah Dollah, Nik Raikhan Nik Him, Fauziah Marpani

Faculty of Chemical Engineering, Universiti Teknologi Mara, 40450 Shah Alam, Selangor, Malaysia

*Corresponding Author: E-mail: nurhidayati0955@uitm.edu.my

Tel: +60 355448027

Abstract

In this study, the potential of graphene oxide-alginate beads (GO-AB) as an adsorbent for bisphenol A (BPA) removal from aqueous solution was investigated. GO was first prepared via modified Hummers' techniques and aerogel alginate bead with embedded GO was prepared using an extrusion dripping method, where calcium chloride was utilized as a curing agent. The physicochemical characteristics of GO-AB were investigated using XRD, FTIR, BET, TGA. The results revealed that crystal structure and the surface groups of GO and alginate were retained upon formation of GO-AB. A batch adsorption testing was carried out as a function of pH (3, 7, and 9), contact time (up to 420 mins) and initial concentration of BPA (50 - 200 $mg \cdot L^{-1}$). The adsorption rate was typically faster at the beginning of the adsorption process and started to level off after 180 mins. AB and GO-AB had better adsorption performances at neutral condition (pH 7) as compared to alkaline and acidic environments owing to repulsive electrostatic interaction between BPA and the adsorbent surface's charge. The sorption kinetic

data was observed fitted to the pseudo-second-order kinetics model (R^2>0.98) and obeyed the Freundlich isotherm model adsorption behaviour as compared to Langmuir. However, the R_L value of Langmuir model is between 0 to 1, which implies favourable adsorption process. The maximum BPA adsorption capacity for AB and GO-AB was found to be 250.00 and 384.62 $mg \cdot g^{-1}$, respectively indicating that GO-AB is a promising adsorbent for BPA removal from aqueous solution.

Keywords: *alginate; graphene oxide; BPA; adsorption; wastewater treatment*

1. Introduction

Bisphenol A (BPA) is among the most utilized monomer in production of various polymers such as epoxy resins, polycarbonates, polysulfone (PS) resins and other types of plastics (Yang et al. 2011; Seachrist et al. 2016; Almeida et al. 2018). It is a potentially harmful substance as it can cause endocrine disruption due to weak estrogenic, antiandrogenic, and antithyroid activities (Ohore and Songhe 2019). Besides industrial wastewater, the contamination of BPA has been found in other water sources such as surface water and ground water (Petrie et al. 2019). As a result, it is essential to control BPA contamination in water resources.

Owing to the hydrophobic properties BPA, adsorption is considered the most appropriate technology to remove BPA from aqueous sources (Xu et al. 2012; Park et al. 2014; Bhatnagar and Anastopoulos 2017). Adsorption is an adhesion process of atoms, ions, or molecules from liquid, gas or dissolved solid, which creates an adsorbate film on the surface of adsorbent(Sophia A. and Lima 2018). It is one of the water remediation technique that has been widely utilised due to versatility of the process, higher removal rate of chemical pollutants, simple setup, relatively low cost, simple operation, and produces minimal harmful secondary products (Ersan et al. 2017). However, the properties of adsorbent are vital in

enhancing adsorption performances. The adsorbents should possess high adsorption capability, rapid adsorption rate, and specific surface reactivity.

Sodium alginate is a natural polymer or polysaccharide with abundance of carbonyl groups, hydroxyl groups and oxygen atom. As a result, alginate possess many distinct characteristic such as highly hydrophilic, biodegradable, and gel-forming abilities making it suitable to be utilized as adsorbent (Martínez-Gómez et al. 2018). Many studies have confirmed that the high removal performance of alginate for chemical pollutants mainly depends on the high content of carboxyl acid groups (Wu et al. 2017). Alginate is also known as an eco-friendly adsorbent that can be easily cross-linked and hardened with ions such as calcium ions (Gao et al. 2020). However, it tends to have weak mechanical strength, particularly as a self-standing material and low thermostability. This has significantly restricted the application of alginate-based materials as adsorbent. Physical or chemical modification such as surface grafting and cross-linking are typically required to boost the applicability of alginate as adsorbent.

Graphene oxide (GO) is a nanoscale carbon that can was firstly isolated via a micromechanical cleavage. It can be synthesized through oxidation and exfoliation of cheap graphite, forming a monomolecular graphite layer with numerous oxygen-containing functionalities such as hydroxyl, carbonyl, carboxyl, and epoxide groups. As a result, GO exhibits many unusual and fascinating physical, chemical, thermal and mechanical properties (Junaidi et al. 2020). Due to many oxygen functionalities on GO planes, it can be easily dispersed in various solvents for further modification or react with many chemical groups to enhance the properties of GO and create new functionalities (Nie et al. 2015). GO have been widely investigated for various applications including sensor, drug delivery and adsorbent for gas and water pollutants. In addition, due to its high theoretical specific surface area, excellent hydrophilicity and mechanical strength, GO is deemed suitable as adsorbent. Recently, GO

has been utilized to improve the performance of alginate-based material particularly sodium alginate(Zhou et al. 2018; Gao et al. 2020)and calcium-alginate (Li et al. 2013; Tian et al. 2020) for wastewater treatment. It was observed that besides improving the thermal stability and mechanical properties, the adsorption capacity of GO-alginate-based adsorbent increased significantly (Platero et al. 2017b). This is because the alginate can act as a scaffold material and also a template for 3D porous structure, while GO acts as a reinforcing filler/linker to connect and strengthen the composite network. Yang et al.(2018) prepared double network graphene oxide/sodium alginate(GO/SA) hydrogels and the adsorption of Mn(II) was noticed to be better (56.49 $mg \cdot g^{-1}$) as compared to other adsorbents. In additions, the GO/SA hydrogels have better thermal stability and biocompatibility due to GO and SA, respectively. Feng et al. (2017) utilized sodium alginate as a template to create a 3D porous network structure with an aim to inhibit the restacking and agglomeration of rGO. The rGO-SA was then used as adsorbent for phenol, BPA and tetracycline. The adsorption of arsenic (As)) and tetracycline (TC) heavy metals on yttrium-immobilized-graphene oxide-alginate hydrogel (Y-GO-SA) was investigated by He et al.(2020) and maximum adsorption capacities up to 273.39 $mg \cdot g^{-1}$ for arsenic and 477.9 $mg \cdot g^{-1}$ for tetracycline were observed. These capacities were higher than other reported adsorbents due to electrostatic interaction, H-bonds, $\pi - \pi$ EDA interaction, n-π EDA interaction, and cation-bonding bridge effects of pollutants with adsorbent.

In this work, sodium alginate bead (AB) and composite graphene oxide-alginate bead (GO-AB) were prepared and used to adsorb BPA from aqueous solution (**Fig. 1**). Although the development of composite GO-alginate based adsorbent have been widely investigated, to the best of our knowledge not many studies have utilized the GO-AB in beads form for BPA removal. The prepared AB and GO-AB adsorbents were first characterized followed by adsorption evaluation studies based on equilibrium and kinetics perspectives. In addition, the influence of pH, operating time, and initial concentration of BPA towards adsorption

performances was investigated in this work.

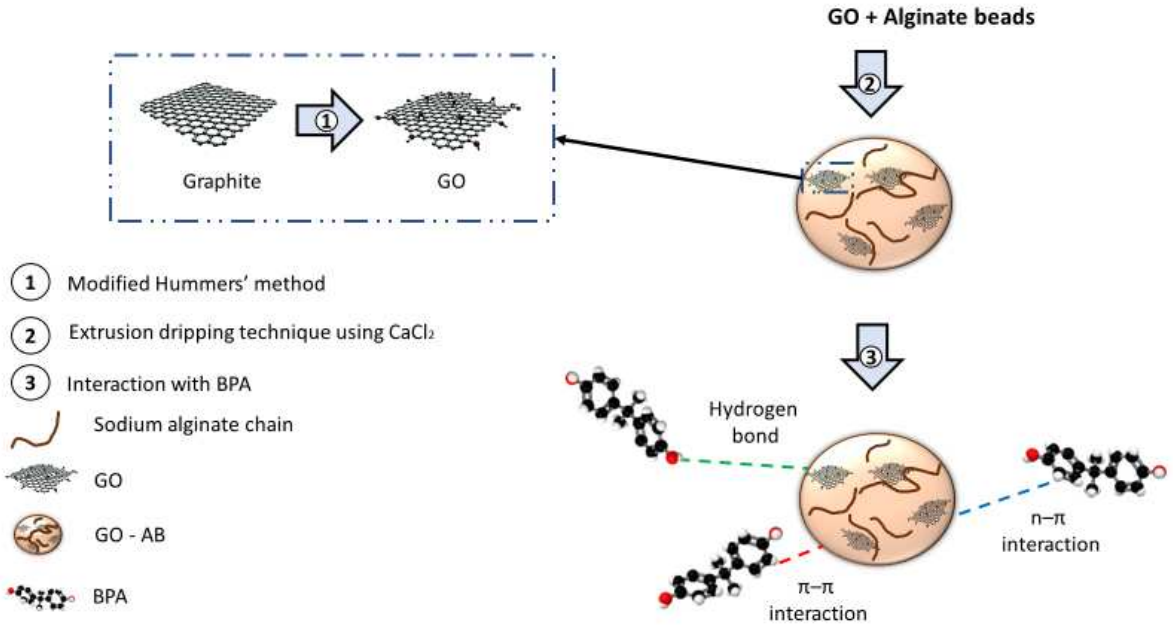

Fig. 1: The schematic diagram of interaction between GO and alginate forming GO-alginate beads (GO-AB)

2. Methodology

2.1 Chemicals and materials

Graphite and Bisphenol A (BPA) were purchased from Merck. Sodium nitrate ($NaNO_3$, MW 84.99 g/mol) and acetone were supplied by Systerm Chemical. Sodium alginate ($C_6H_9NaO_7$, MW 250,000 g·mol^{-1}), calcium chloride ($CaCl_2$), hydrogen peroxide (H_2O_2, 35%), potassium permanganate ($KMnO_4$, MW 158.03 g·mol^{-1}), hydrochloric acid (HCl) and sulfuric acid (H_2SO_4, 98%) were obtained from R&M Chemical. Deionized (DI) water was used in all the experimental work.

116 *2.2 Preparation of GO*

117 GO was synthesized through oxidation and exfoliation of graphite powder based on our
118 previous method (Othman et al. 2017, 2018). The resulting GO solution was left to cool down
119 after reaction termination before continually washed with diluted HCl and DI water. The
120 neutral solution was then centrifuged at 10 000 rpm and 25 °C for 25 min. The supernatant
121 obtained after centrifugation was filtered and the dried in an oven at 60 °C for 24 h to collect
122 GO powder.

123

124 *2.3 Synthesis of GO-AB aerogel beads*

125 Extrusion dripping technique using $CaCl_2$ as a curing agent was utilized to produce alginate
126 aerogel beads. First, 2.3 g of sodium alginate was added into 150 mL of distilled water and
127 stirred vigorously for 3 h. Then, 1.5 wt% of GO suspensions was added to the sodium alginate
128 solution and continually stirred until a homogenous solution of GO-alginate was obtained.
129 After that, the alginate/GO solution was extruded through an 0.55 mm injection needle u into
130 the solution of 0.1 wt % of $CaCl_2$ gelling solution using a syringe pump. The gap between the
131 surface of the $CaCl_2$ solution and the surface of the needle was maintained at 10 cm to ensure
132 the uniformity of the beads shape. After the aerogel GO-AB was formed, it was kept in the
133 $CaCl_2$ solution with minimal agitation for 3 h (**Fig. 2**). In order to ensure complete gelation, the
134 GO-AB was left overnight in $CaCl_2$ solution at 4 °C. The GO-AB was filtered, rinsed with DI
135 water, and allowed to dry in an oven at 40 °C until constant weight.

136

Fig. 2 Photograph of extruded aerogel beads in $CaCl_2$ solution

2.4 Characterization

X-ray diffraction (XRD) was utilized for structural characteristics study of the synthesised GO-AB aerogel beads. The XRD pattern was recorded using X'celerator detector (Rigaku) where Cu Kα was used as the radiation source. The equipment voltage and current were set at 40 kV and 40 mA, respectively. The sample was scanned within the scan range of 2θ of 5° to 90° at a scan step width of 0.05°. Fourier transform infrared spectroscopy (FTIR, Perkin Elmer) was utilized to identify organic functional groups where the scan was carried out from 600–4000 cm^{-1}. Thermogravimetric analysis (TGA) was performed to measure the thermal stability of adsorbents prepared using Mettler Toledo analyser. A heating rate of 10 °C·min^{-1} was used, and the weight loss profile was recorded at a temperature range of 25 to 1000 °C. The specific surface area and pore volume of adsorbents were analyzed using an automated gas sorption system through nitrogen adsorption and desorption system using Brunauer, Emmett, and Teller (BET) NOVA 1200e surface area and pore size analyzer (Quantachrome Instrument).

2.5 Batch BPA adsorption experiments

Adsorption capacity and BPA removal efficiency of composite GO-AB aerogels for the

removal of BPA were examined using a batch experiment under a stirring speed of 150 rpm where the pH solution and BPA concentration were varied. The influence of pH was investigated by adding 0. 1 g of adsorbent with 200 mL (0.5 $g \cdot L^{-1}$) of 50 $mg \cdot L^{-1}$ of BPA concentration under constant stirring at 30 °C up to 420 mins. The working solution of BPA was prepared by first dissolving solid BPA in ethanol due to BPA's low solubility in water. Then, it was diluted into the required concentrations using DI water in an Erlenmeyer flask. 0.1 M hydrochloric acid (HCl) or 0.1 M sodium hydroxide (NaOH) was then added to adjust the pH of BPA solutions.

The effects of initial BPA concentration were investigated using 50, 100, 150, and 200 $mg \cdot L^{-1}$ of BPA solutions. After adsorption, the supernatant was taken out by using a syringe and UV–visible spectrophotometer (Hach DR2800) at 276 nm was used to measure the concentration. The adsorption capacity, q_t ($mg \cdot g^{-1}$) and removal efficiency (%) were determined using Eq. (1) and Eq. (2), respectively.

$$q_t = \frac{(C_0 - C_t)V}{m} \quad (1)$$

$$Removal\ efficiency\ (\%) = \frac{(C_0 - C_t)}{C_0} \times 100 \quad (2)$$

where the C_0 and C_t are the BPA initial concentration and concentration at time t ($mg \cdot L^{-1}$), respectively, V is the volume of solution (L), and m is the mass of the adsorbent (g). The testings were conducted in triplicates, and the results are depicted as mean values.

The adsorption kinetics offers vital knowledge on the adsorption rate and mechanism. This kinetic study can be further used to design and adsorption unit. Two kinetics models i.e pseudo-first-order and pseudo-second-order were used to examine the mechanism of BPA adsorption. The linear form of the pseudo-first-order model is determined by Eq. (3):

$$log\,(q_e - q_t) = log\,q_e - (\frac{K_1}{2.303})t \quad (3)$$

where K_1 is the first-order rate constant (min^{-1}), and q_e and q_t are the quantities of adsorbed BPA ($mg \cdot g^{-1}$) at equilibrium and at time t (min). The straight-line plot of log ($q_e - q_t$) against t gives log (q_e) as slope and intercept equal to K_1 /2.303. The linear form of the pseudo-second-order model is given by Eq. (4):

$$\frac{t}{q_t} = \frac{1}{K_2 q_e^2} + \frac{1}{q_e} t \quad (4)$$

where K_2 is the pseudo-second-order rate constant ($g \cdot mg^{-1}min^{-1}$) and can be determined from the intercept of the plot of t/q_t versus t.

3. Results and Discussion

3.1 Formation of aerogel AB and GO-AB

Fig. 3 shows the resulting AB and GO-AB aerogels formed through the extrusion process. In general, they have a uniform spherical shape. After drying overnight in an oven at 40 °C, the size of the aerogels decreased by 10%–20% while maintaining the spherical shape. This shows that the drying method of gel beads affects their size without changing their shapes (Platero et al. 2017a). The size of AB and GO-AB decreased from 2.90 to 2.60 and 3.20–2.35 mm after drying, respectively. The extruded GO-AB beads were generally bigger than AB due to the high viscosity of GO-AB solution owing to the addition of GO. As the GO-AB solution was viscous, the attraction forces are stronger, thus forming bigger particles (Ganesan et al. 2018). However, after the drying process, GO-AB tended to have smaller particles than GO. The decrease in the aerogel size was due to the moisture removal and surface tension on the gel

beads during oven-drying. However, low drying temperature was utilised to avoid damage on the aerogel surface, shape, and nature.

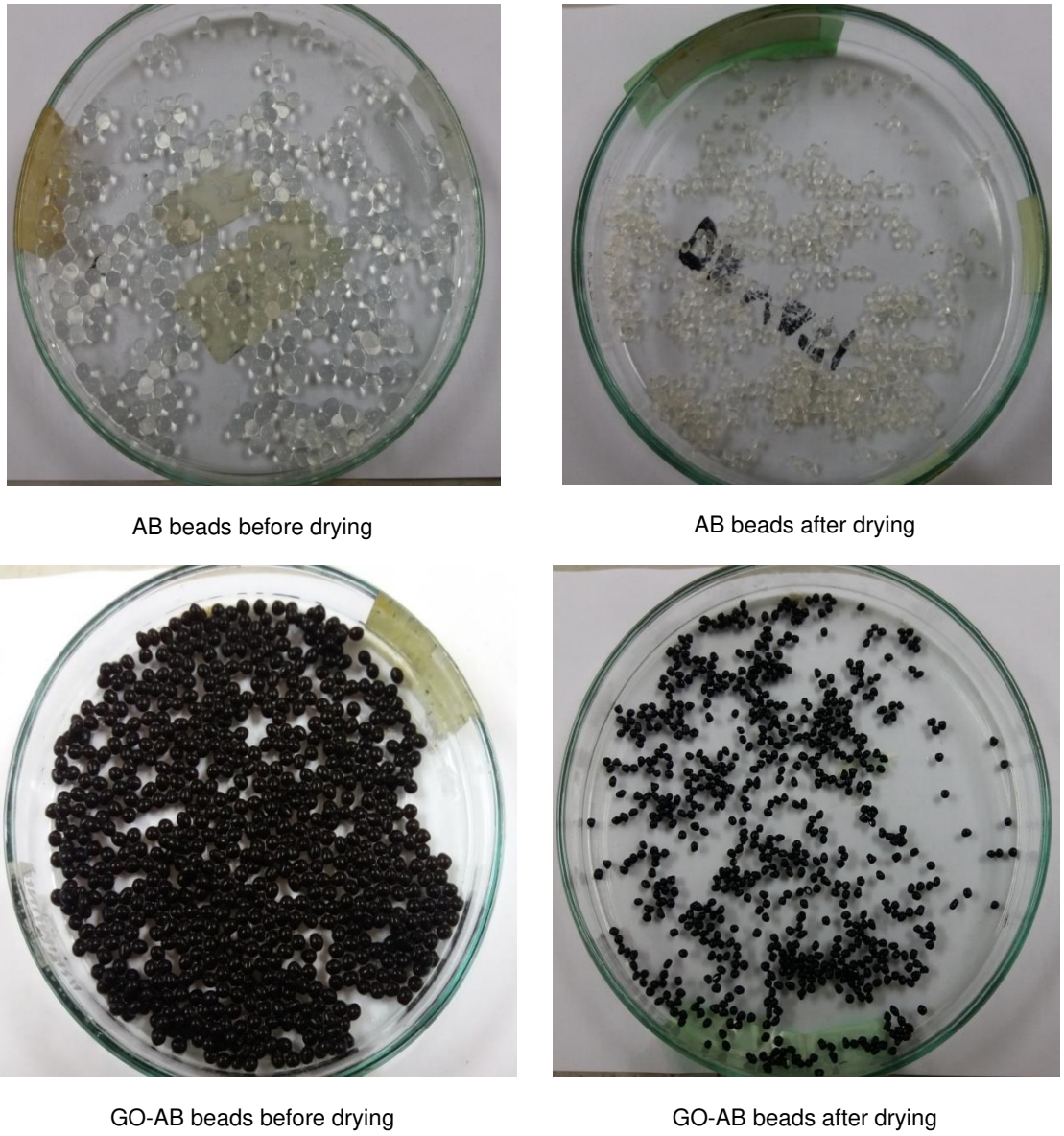

Fig. 3 Photograph of alginate bead (AB) and graphene oxide-alginate beads (GO-AB) prepared in this work, before and after drying.

3.1 Characterization of GO, aerogel AB and aerogel GO-AB

The XRD patterns of GO, AB, and GO-AB are shown in **Fig. 4**. The characteristic diffraction peak of GO was observed at 2θ = ~10°, which corresponded to the 002 plane and consistent

with others finding (Ionita et al. 2013; Nie et al. 2015; Wang et al. 2017). The peaks indicate the existence of oxygen-containing group and further confirmed that the graphite was fully oxidized into GO. Sodium alginate is typically amorphous with a distinct diffraction peak at 2θ= ~13°. As the alginate beads (AB) has been crosslinked with calcium chloride, the crystallinity of AB was observed to increase, which further confirms the interaction between sodium alginate and calcium chloride (Grossi et al. 2014). As for GO-AB, the diffraction pattern was found to be consistent with the XRD pattern of AB where no distinct difference for alginate bead (AB) and after GO addition (GO-AB). This confirms that GO was evenly dispersed and the addition of GO has minimal impact on the crystallinity of GO-AB (Sun and Fugetsu 2014). This also indicates that excellent intermolecular interaction between GO and AB, which provides good miscibility for preparation of GO-AB aerogels (Jiao et al. 2016).

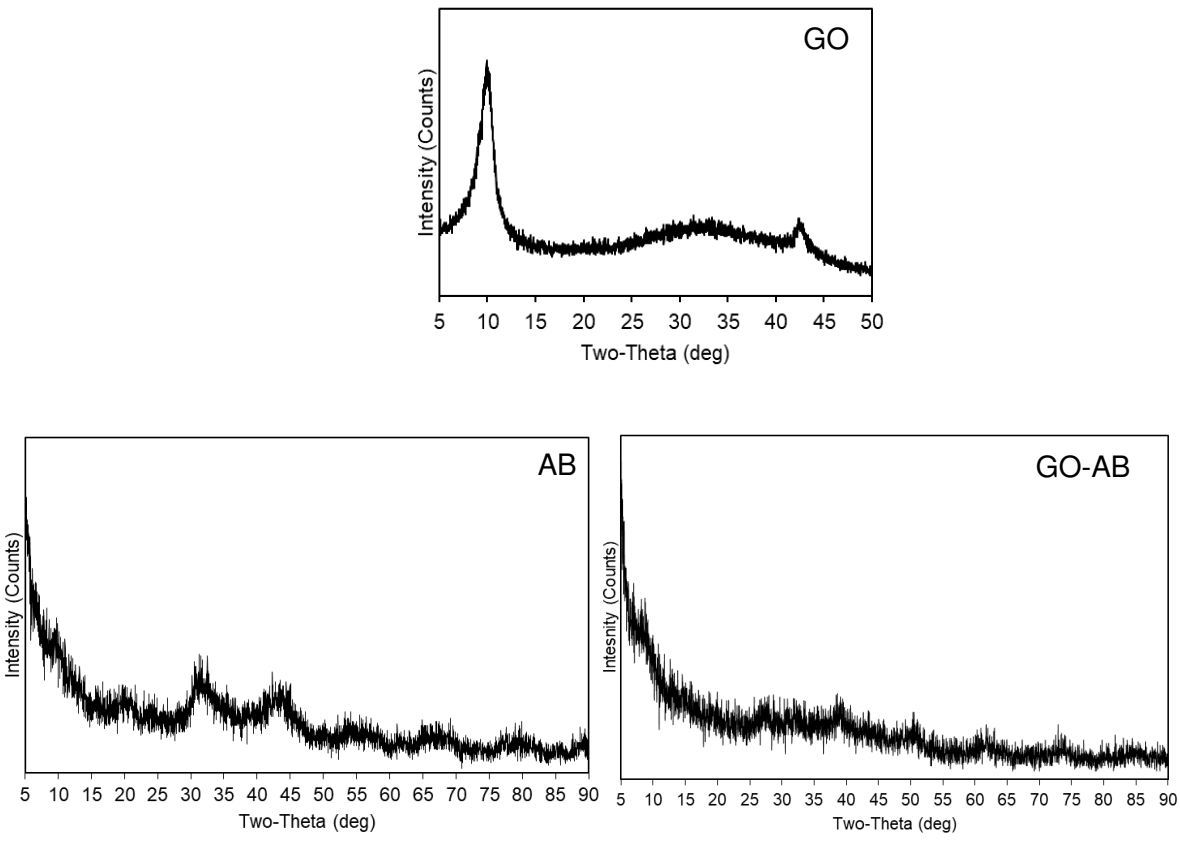

Fig. 4 XRD spectra of GO, AB, and GO-AB

The FTIR spectra of GO, AB, and GO-AB are presented in **Fig. 5** and the spectra are typically comparable to the ones previously reported (Ionita et al. 2013; Nie et al. 2015; Jiao et al. 2016; Platero et al. 2017a). In general, the wide band spectra in the range of 3600–3100 cm^{-1} indicate the presence of hydroxyl group peaks, and the lower wavelengths present oxygen-containing groups, such as carbonyl and epoxides (Co et al. 2017). The characteristic peaks of GO were observed at 3353, 1714, 1623, and 1094 cm^{-1}, which validates the existence of hydroxyl (O–H) stretching vibration, carboxylic group (C=O) stretching vibration, C=C stretching mode of sp^2 network, and C–O group stretching vibration, respectively. This confirmed the successful of oxidation and exfoliation of graphite to GO (Nie et al. 2015).

The FTIR spectra of AB show several characteristics peaks at 3341, 1608, 1433, and 1021 cm^{-1} that indicate the presence of hydroxyl (O–H) stretching vibration, symmetric and asymmetric stretching vibrations of carboxylate salt group (C–O–O), and stretching vibration of C–O–C group, respectively (Ionita et al. 2013). The C–H stretching vibration observed for AB at 939 and 884 cm^{-1} signifies uronic acid and mannuronic acid, respectively. The FTIR spectra of GO-AB shows the presence of both characteristics peaks of AB and GO, with no apparent changes as compared to AB. This further confirms that GO-AB was successfully prepared in this work.

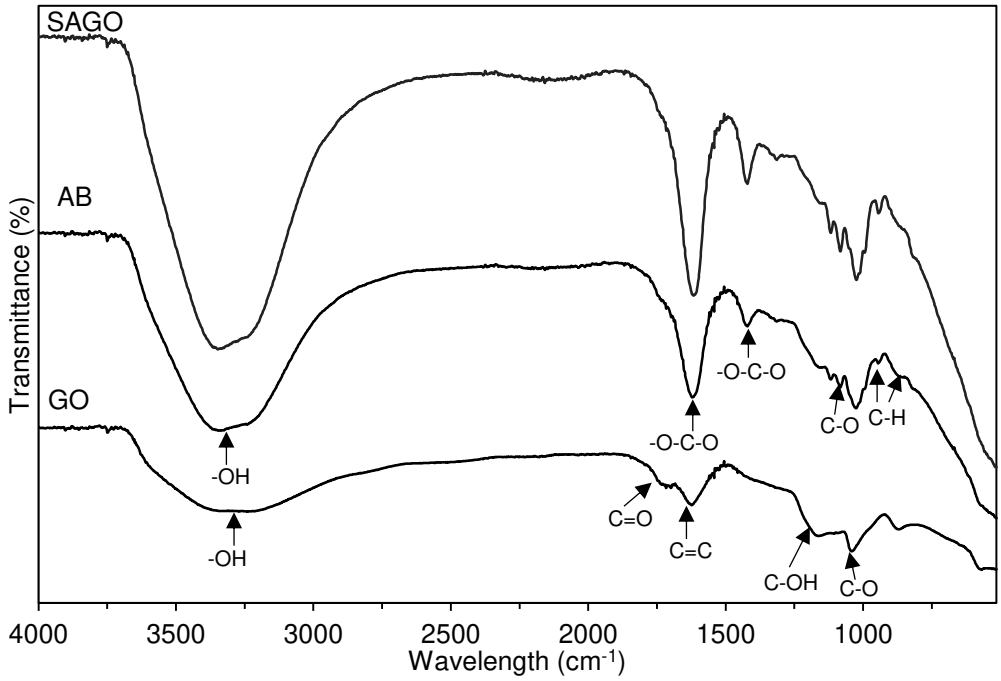

Fig. 5 FTIR spectra of GO, AB, and GO-AB aerogels.

Fig. 6 displays the thermal stability of GO, AB, and GO-AB at room temperature until 500 °C. GO had better stability than AB and GO-AB, particularly at the beginning of the heating process. GO lost only 10% of its mass at a temperature below 180 °C and up to 60% from 180 to 200 °C. In comparison, AB and GO-AB were not stable and started to lose mass rapidly at the beginning of the heating up process up to 80% and 60%, respectively. The weight losses at the beginning of analysis was mainly due to the evaporation of free water from the AB and GO-AB (Fei et al. 2016). As the temperature increased up to 220 °C, the observed weight losses were probably due to the removal of hydrated water. Then, the alginate chains start to break and possible disintegration of GO fractured and GO disintegrated. At approximately 300 °C, the mass loss of AB and GO-AB started to stabilise, giving a total mass loss of 83% and 74%, respectively. It can be concluded that GO-AB was more stable than AB, which suggests that the movement of AB chains was hindered by strong electrostatic interaction with GO leading to better thermal stability of GO-AB.

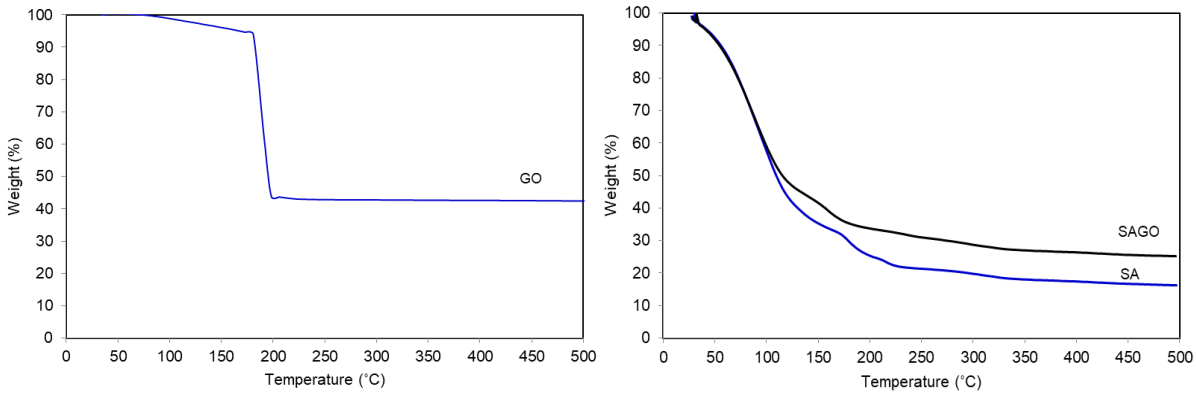

Fig. 6 TGA of GO, AB, and GO-AB

The N_2 adsorption–desorption isotherm and measurement of AB and GO-AB and summarises are shown in Fig. 7 and Table 1. The adsorption and desorption of N_2 increased rapidly, and both the AB and GO-AB isotherms can be classified as type IV isotherm based on the International Union of Pure and Applied Chemistry (IUPAC) classification (Hwang and Barron). Type IV isotherm is normally for the ordered mesoporous materials i.e materials with pore diameter between 2 and 50 nm, which is consistent with the average pore diameter obtained in the work (Fei et al. 2016). The BET surface areas of AB and GO-AB obtained in this work were 51.28 and 7.19 $m^2 \cdot g^{-1}$, respectively, while the average pore diameters of AB and GO-AB were 12.14 and 24.52 nm, respectively. These values were comparatively higher than an earlier reported value (0.2-2.6 $m^2 \cdot g^{-1}$ and 1.3-2.8 nm)(Yang et al. 2018) although the amount of GO added into the alginate solution in this work was smaller. Although the surface area of adsorbent reduced with the addition of GO, the pore diameter shows a different trend. A bigger pore diameter was observed for GO-AB, which was contradicted with the findings by Fei et al.(2016) where the addition of GO tends to increase the surface area and reduce the pore diameter. As pore size plays a vital role in adsorption performance, in which adsorbent with

smaller pore size typically fails to capture larger adsorbates (Chowdhury et al. 2013), GO-AB might have better performance than AB.

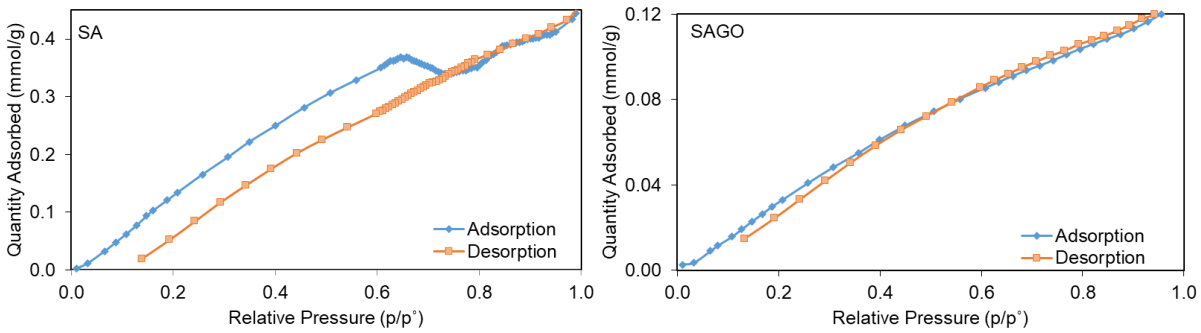

Fig. 7 Nitrogen adsorption –desorption measurement of AB and GO-AB adsorbents

Table 1. BET analysis of AB and GO-AB adsorbents

Sample	Specific surface area ($m^2 \cdot g^{-1}$)	Average pore diameter (nm)
AB	51.28	12.14
GO-AB	7.19	24.52

3.2 Adsorption study for BPA

3.2.1 Effects of initial pH solution towards BPA removal

The pH of the aqueous solution can significantly affect the adsorption performances as it could alter the charge density of the adsorbent surface and the concentration of dissolved ions in the solution (Zhao et al. 2018). The effect of pH towards the removal rate and adsorption capacity of 50 $mg \cdot L^{-1}$ BPA was investigated at 30 C°. **Fig. 8** shows the adsorption performances of BPA at different pH values for AB and GO-AB. The removal efficiency of BPA increased with time and nearly reached a plateau after approximately 180 min. This is assumed as equilibrium time at which adsorption occurred. At the start of adsorption, the removal efficiency was greater owing to the high active sites' availability of the adsorbent. Then, it decreases with time

because of saturation of BPA and reduction of the adsorbent active sites, which caused removal efficiency declination (Abdel-Gawad and Abdel-Aziz 2019). By comparing the removal efficiency of BPA for AB and GO-AB at each pH value, GO-AB adsorbed more BPA than AB, and consequently leads to higher BPA removal rate up to 85% after 480 mins. Electrostatic interaction is formed among the anions and organic oxygen-containing functional group of the adsorbent surface and hence, the adsorption capacity of adsorbent decreased [32].

The adsorption capacity of GO-AB was greater than AB, where the maximum adsorption capacity was observed at pH=7 (83.33 $mg \cdot g^{-1}$) and reduced to 72 $mg \cdot g^{-1}$ and 65.87 $mg \cdot g^{-1}$ at acidic (pH=3) and alkaline (pH=9) environments, respectively. Low adsorption capacities were observed at low and high pH values due to the competitive adsorption between H^+, OH^- ions, and BPA molecules. Rapid decrease of adsorption capacity at pH=9 might be cause by adsorption inhibition in the strong alkaline environment. BPA is a neutral molecule and forms divalent anions at around pH 9.56 (Bhatnagar and Anastopoulos 2017). The pKa of BPA is 9.6 –10.2 , and thus BPA can be ionized in pH from 9-10 which increases the formation of bisphenolate anions (Liu et al. 2018). Li et al. (2015) investigated the effects of pH towards adsorption of BPA using HTAB-bentonite and found that there was a slight increase of BPA between pH 4-7, while tat pH>7, a significant decrease of BPA removal was observed. Similar findings have been observed by Guo et al.(2011) where the adsorption capacity of BPA reduced significantly when the pH value is greater than 7. According Liu et al.(2016), molecular form of BPA started to deprotonated at pH 8.0 - 9.0, which caused the ionization of BPA molecules into mono- or divalent anions. As a results, a repulsive electrostatic interaction of organic oxygen-containing functional group or negatively charged adsorbent surface was formed with bisphenolate anion (Peng et al. 2017; Bhatnagar and Anastopoulos 2017). In addition, the alkaline solution might contain more sodium cations (Fei et al. 2016), which can affect the surface properties of AB and GO-AB and therefore reduces the adsorption capacity. At lower

pH, there might also be an excess of H^+ ions competing for adsorption sites. Hence, this indicates that the adsorption of BPA should be conducted in a neutral environment. The fast adsorption rate and high adsorption capacity demonstrated that GO-AB was an efficient adsorbent for the adsorption of BPA.

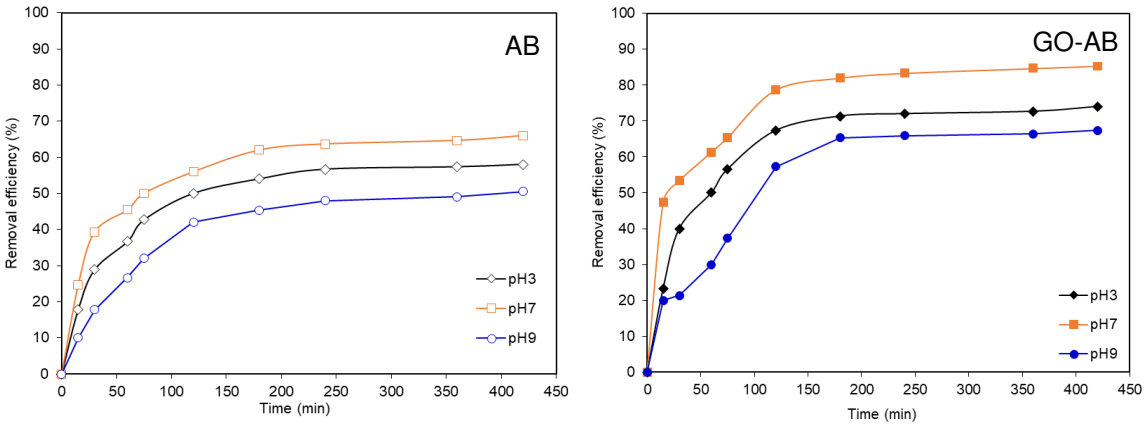

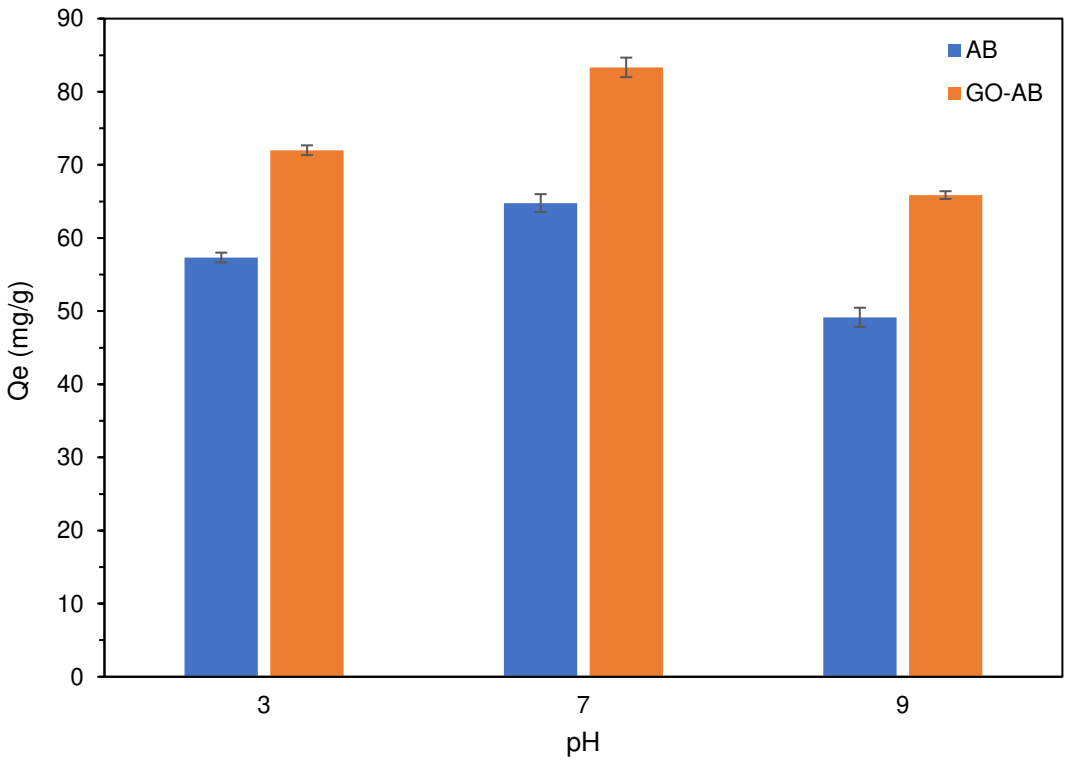

Fig. 8. Removal efficiencies and adsorption capacities of AB and GO-AB towards BPA at pH values of 3, 7, and 9 (Mass of adsorbent and initial concentration of BPA were fixed at 0.5 $g \cdot L^{-1}$ and 50 $mg \cdot L^{-1}$, respectively)

334

335 *3.2.2 Effect of initial concentration of BPA solution*

336 The effect of initial BPA concentration on the BPA removal was evaluated using 0.1 g of
337 adsorbent in 200 ml of BPA solution and the solution was kept at pH of 7. In Fig. 9, it can be
338 seen that as the initial concentration of BPA increased, the removal efficiency decreases. At
339 50 $mg \cdot L^{-1}$, the removal efficiency was higher due to the availability of accessible pores in AB
340 and GO-AB. As the BPA concentration increases, the active sites or pores of AB and GO-AB
341 adsorbent was not sufficient to adsorb more BPA compound and became saturated. As a result,
342 the BPA could not be taken by the adsorbent, thus, reducing the removal efficiency of the
343 adsorbent (Huang and Wang 2018). These results were in accordance to other previous works
344 (Liu et al. 2018; Martín-Lara et al. 2020). It should be noted that when the BPA
345 concentration was higher than 100 $mg \cdot L^{-1}$, the BPA removal (%) was not substantially
346 influenced by the initial BPA concentration. This might indicate that the adsorbent surface
347 reach the saturation point.

348 In term of equilibrium capacity of adsorbent, it can be seen that it is positively correlated
349 to the initial BPA concentration in the aqueous solution. The adsorption capacity of BPA for
350 AB and GO-AB increased from 66 to 203 $mg \cdot L^{-1}$, and 85.33 to 267.33 $mg \cdot L^{-1}$, respectively
351 with a rise in the initial BPA concentration from 50 to 250 $mg \cdot L^{-1}$. The key reason for this is
352 the increase in driving force to overcome the mass transfer resistance between aqueous and
353 solid phases (Ahmaruzzaman 2011; Pathania et al. 2017; Fraga et al. 2019). Overall, the
354 removal efficiency of GO-AB was better than that of AB due to the porosity of GO-AB
355 adsorbent and availability of oxygen-containing functional group on the surface of GO, which
356 offered additional strong surface complexion of BPA (Algothmi et al. 2013).

357

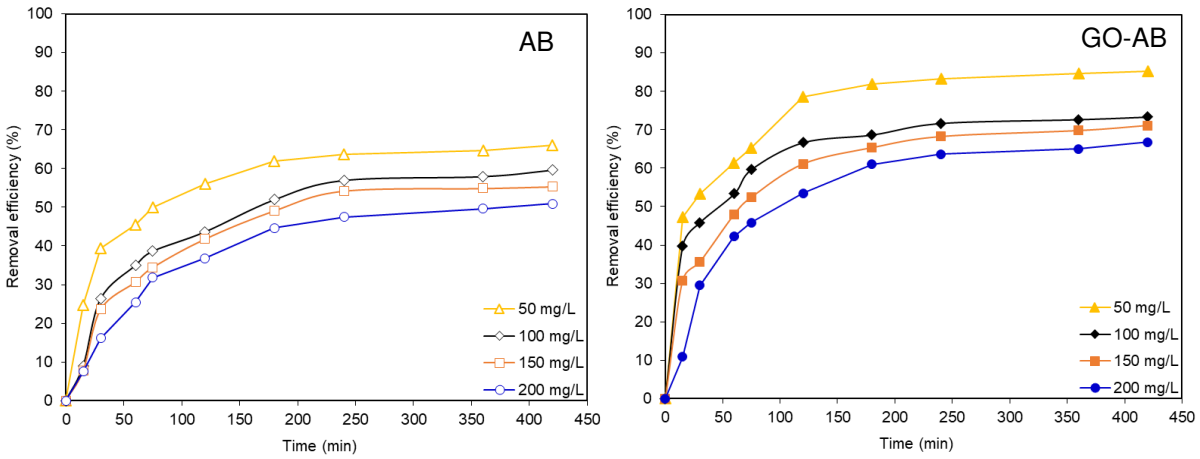

358

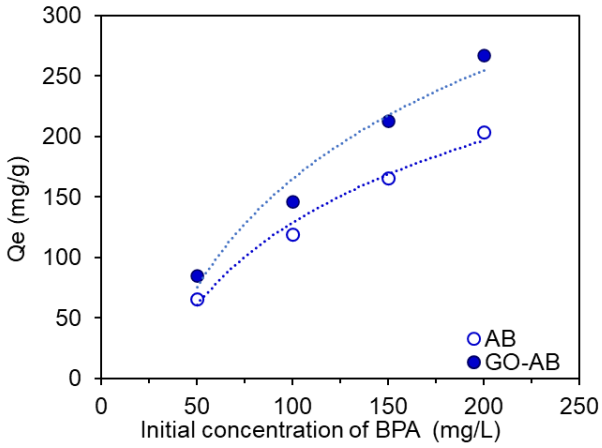

359

360 **Fig. 9** Effects of BPA initial concentrations (C_0=50, 100, 150, and 200 50 mg·L^{-1}) on adsorbent
361 performances in term of removal efficiency and adsorption capacity (Mass of adsorbent and
362 pH were set at 0.5 g·L^{-1} and 7, respectively.

363

364 *3.3 Adsorption Kinetics*

365 The results of pseudo-first-order (PFO) and pseudo-second-order (PSO) adsorption kinetics
366 data fitting are listed in **Fig. 10** and **Table 2.** The linear form of the PFO model is generally
367 appropriate for lower concentrations of solute. It can be seen that the values of R^2 for PFO
368 model are lowered for most of the adsorption data, which indicates that the BPA adsorption
369 onto AB and GO-AB does not obey the PFO kinetic model. The rate of PSO reaction is
370 dependent on the amount of solute adsorbed on the adsorbent surface and the amount adsorbed
371 at equilibrium. This indicates that the rate-limiting step in PSO is the chemisorption-surface

adsorption and the adsorbate removal rate is highly depending on the physicochemical interactions between the two phases. In general, the correlation coefficients show that the adsorption kinetic data for BPA onto AB and GO-AB were better associated by the PSO model, where the value of R^2 is greater than 0.99. Several works on the adsorption of BPA onto various adsorbents noticed similar trend (Acosta et al. 2018; Wang and Zhang 2020; Lazim et al. 2020). According to the PSO model, boundary layer resistance is not the rate-limiting step. The external resistance model cannot satisfactorily explain the adsorption mechanism. Thus, it can be assumed that the overall mechanism of BPA adsorption was chemisorption, and the rate-controlling step involves valence forces via exchange and share of electrons between BPA molecules and the adsorbent.

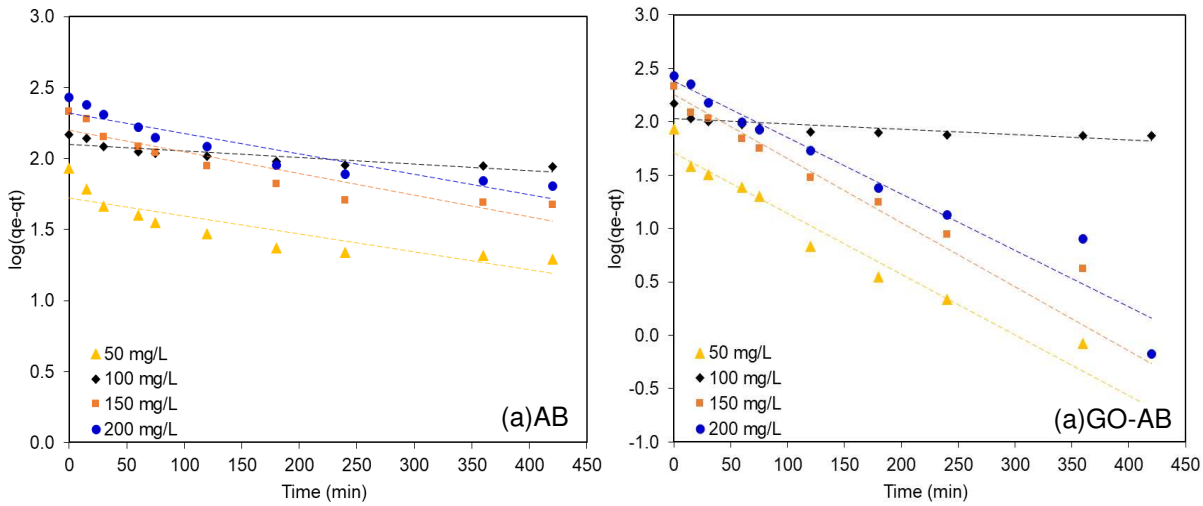

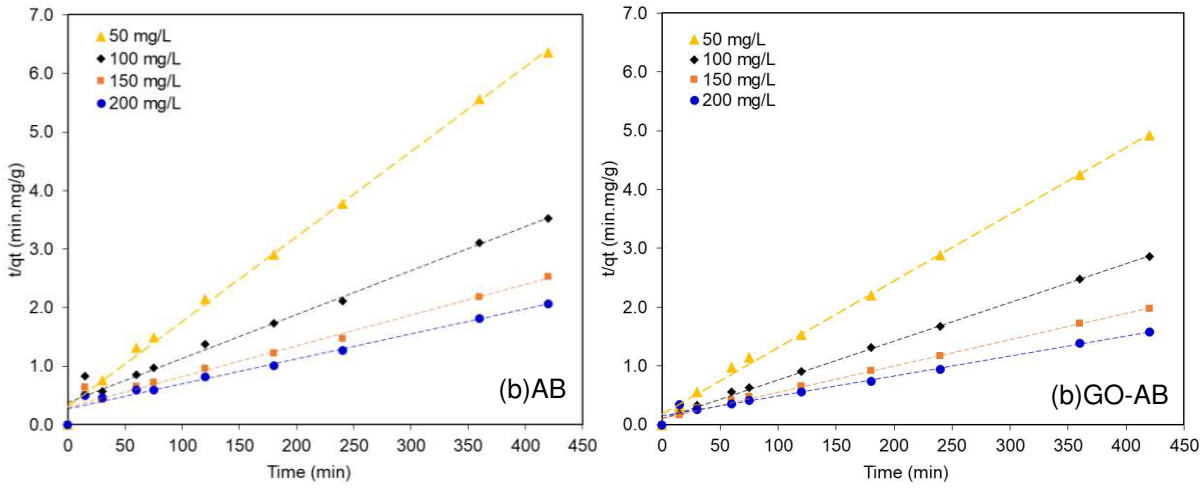

Fig. 10 Experimental kinetics data (a) pseudo first order (PFO) and (b) pseudo second order (PSO) for the adsorption of BPA by AB and GO-AB. The dotted lines show the predicted values of the best-fitted model.

Table 2. Kinetic parameters of the pseudo-first order (PFO) and pseudo-second order (PSO) models for BPA adsorption on AB and GO-AB

Adsorbent	Conc. ($mg \cdot L^{-1}$)	Pseudo-first-order			Pseudo-second-order		
		Q_e ($mg \cdot g^{-1}$)	K_1 x10^3 (min^{-1})	R^2	Q_e ($mg \cdot g^{-1}$)	K_2 x10^4 ($g \cdot mg^{-1} \cdot min^{-1}$)	R^2
AB	50	52.76	2.9939	0.7532	68.97	6.6950	0.9965
	100	126.44	1.1515	0.7663	133.33	1.4850	0.9755
	150	159.26	3.4545	0.8556	188.68	0.9659	0.9694
	200	209.60	3.2242	0.8779	232.56	0.6873	0.9697
GO-AB	50	51.11	13.1271	0.9713	88.50	7.1169	0.9974
	100	106.54	1.1515	0.5971	151.52	4.2745	0.998
	150	179.14	13.8180	0.9233	222.22	1.9304	0.9958
	200	238.73	12.2059	0.9233	294.12	0.7885	0.9806

3.4 Adsorption Isotherm

Adsorption isotherm is crucial to establish the adsorption behaviour and to forecast the favourability of the adsorption system. The adsorption data were then analyzed by fitting to Langmuir and Freundlich isotherm models. Langmuir isotherm model presumes that maximum adsorption is corresponded to formation of monolayer adsorbate on the adsorbent surface due to chemisorption. However, when the adsorption reaches the equilibrium, no further adsorption can happen owing to the limited adsorption sites. At this point, the energy of adsorption is constant, and no transmigration of adsorbate occurs on the surface. The linearised form of the Langmuir isotherm model can be expressed in Eq. (5):

$$\frac{C_e}{q_e} = \frac{1}{K_L Q_m} + \frac{C_e}{Q_m} \quad (5)$$

where C_e (mg·L^{-1}) is the concentration at equilibrium, Q_e (mg·g^{-1}) is the amount of adsorption at equilibrium, Q_m (mg·g^{-1}) is the maximum monolayer capacity of adsorbent, and K_L (L·mg^{-1}) is the Langmuir adsorption constant. A plot of $1/q_e$ against $1/C_e$ should be linear if the adsorption follows Langmuir behaviour, with a slope of $1/K_LQ_m$ and intercept of $1/ Q_m$. Dimensionless separation factor, R_L is also an essential parameter in Langmuir isotherm that can be calculated as Eq. (6):

$$R_L = \frac{1}{1+K_L C_0} \quad (6)$$

where R_L implies the Langmuir isotherm to be either irreversible ($R_L = 0$), favourable ($0 < R_L < 1$), linear ($R_L = 1$) or unfavourable ($R_L > 1$). The Freundlich isotherm model is an empirical correlation depicting the adsorption of solutes from liquid to solid surface and presumes that multilayer adsorption happens on a heterogeneous surface through weak van der Waals forces. The linear form of the Freundlich is shown in Eq. (7):

$$\boldsymbol{\log q_e = \left(\frac{1}{n_f}\right) \log C_e} + \log K_f \quad (7)$$

where K_f and n are Freundlich constant and heterogeneity factor, respectively, which are determined by the intercept and slope of the linear plot (**Fig. 11**). It can be seen that as the BPA concentration increases, the equilibrium adsorption capacity of both AB and GO-AB adsorbents rises gradually owing to an escalation of BPA chemical potential. The estimated model parameters are summarised in **Table 3.** Owing to the high correlation coefficient ($R^2 > 0.98$), the Freundlich isotherm seems to be a favourable model to describe the adsorption activity, which is initiated by the multi-molecular layer adsorption process. However, the R_L

values of AB and GO-AB obtained through Langmuir model are in the range of 0 to 1, which indicated that the adsorption of BPA on both adsorbents is preferential adsorption. In addition, based on the Q_{max} obtained from the Langmuir isotherm, GO-AB fabricated in this work possessed higher adsorbability (384.62 mg/g), exceeding other adsorbents investigated, making it a potential candidate to remove BPA.

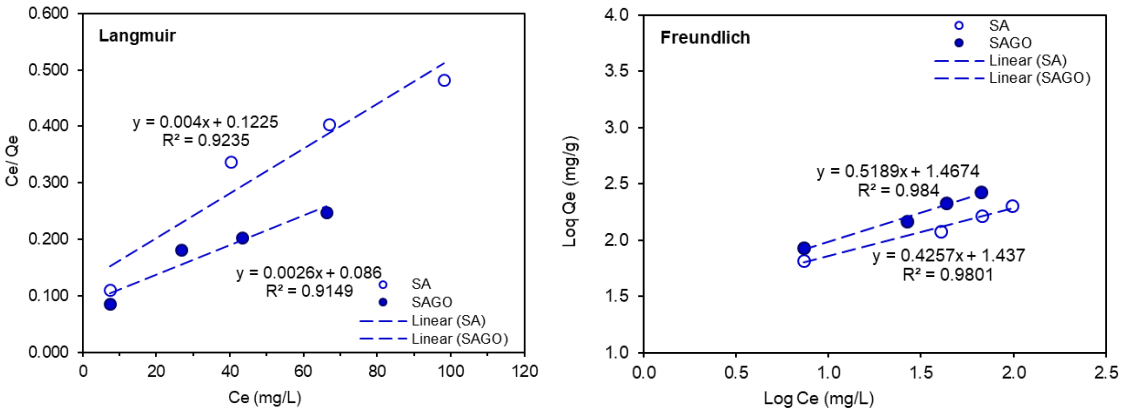

Fig. 11. Langmuir and Freudlich isotherm plots for AB and GO-AB

Table 3. Langmuir and Freundlich parameters for adsorption isotherms of AB and GO-AB aerogel

Adsorption model	Isotherm parameters	AB	GO-AB
Langmuir	K_L (L·mg^{-1})	0.03	0.03
	Q_m (mg·g^{-1})	250.00	384.62
	R_L	0.9997	0.9997
	R^2	0.9235	0.9149
Freundlich	K_f(L·mg^{-1})	27.35	29.33
	n	2.3490	1.9272
	R^2	0.9801	0.984

4. Conclusion

In this work, alginate-based adsorbents (AB and GO-AB) were successfully prepared and characterized. In general, the addition of GO into AB significantly improved the

physicochemical properties of the alginate-based adsorbent through composite networking reinforcement, where GO acts as a crosslinker to strengthen the GO-AB structure. The thermal stability of GO-AB was found to improve due to the suppression of AB chain's mobility by strong electrostatic interaction with GO. The BET result shows that the adsorbent prepared is mesoporous, with an increase of pore diameter for GO-AB. The adsorption of BPA on AB occurred rapidly through the electrostatic interaction and highly depending on pH of aqueous solution. The adsorption behaviour fitted the pseudo-second-order kinetics model and Freundlich model, respectively. The maximum adsorption capacity of AB and GO-AB were 250.00 and 384.62 $mg \cdot g^{-1}$, respectively. This suggests that GO-AB is a promising adsorbent for the removal of BPA from aqueous solution.

Ethics approval and consent to participate

Not applicable.

Consent for publication

All authors have agreed with the content and all have given explicit consent to publish.

Availability of data and materials

The datasets used and/or analysed during the current study are available from the corresponding author on reasonable request.

Competing interests

The authors declare no competing interests.

Fundings

Universiti Teknologi MARA 600-RMC/YTR/5/3 (002/2020).

Authors' contributions

Nurul Syazana Fuzil contributed to sample preparation, carried out the experiments and writing the manuscript.

Nur Hidayati Othman contributed to data analysis, interpretation of the results and lead in writing the manuscript.

Nur Ain Shazwani Roslee Ab. Jamal contributed to sample preparation and perform the experiments.

Nur Hashimah Alias contributed to experimental planning and chemicals purchasing.

Ana Najwa Mustapa contributed to Graphene Oxide-Alginate beads preparation.

'Aqilah Dollah contributed to the sample properties analysis.

Nik Raikhan Nik Him contributed to the interpretation of the results.

Fauziah Marpani contributed to the validation of the results.

All authors provided critical feedback and helped shape the research, analysis and manuscript.

Acknowledgements

The authors would like to express their gratitude to Sharita Fardeyra Mohd Sharip and Nurulfarhana Zulkifli for the assistance given during the experiments. This study was supported by Universiti Teknologi MARA internal grant (600-RMC/YTR/5/3 (002/2020)).

References

Abdel-Gawad SA, Abdel-Aziz HM (2019) Removal of ethinylestradiol by adsorption process from aqueous solutions using entrapped activated carbon in alginate biopolymer: isotherm and statistical studies. Appl Water Sci 9:75. https://doi.org/10.1007/s13201-019-0951-7

Acosta R, Nabarlatz D, Sánchez-Sánchez A, et al (2018) Adsorption of Bisphenol A on KOH-activated tyre pyrolysis char. J Environ Chem Eng 6:823–833. https://doi.org/10.1016/j.jece.2018.01.002

Ahmaruzzaman M (2011) Industrial wastes as low-cost potential adsorbents for the treatment of wastewater laden with heavy metals. Adv Colloid Interface Sci 166:36–59. https://doi.org/10.1016/j.cis.2011.04.005

Algothmi WM, Bandaru NM, Yu Y, et al (2013) Journal of Colloid and Interface Science Alginate – graphene oxide hybrid gel beads : An efficient copper adsorbent material. J Colloid Interface Sci 397:32–38. https://doi.org/10.1016/j.jcis.2013.01.051

Almeida S, Raposo A, Almeida-González M, Carrascosa C (2018) Bisphenol A: Food Exposure and Impact on Human Health. Compr Rev Food Sci Food Saf 17:1503–1517. https://doi.org/10.1111/1541-4337.12388

Bhatnagar A, Anastopoulos I (2017) Adsorptive removal of bisphenol A (BPA) from aqueous solution: A review. Chemosphere 168:885–902. https://doi.org/10.1016/j.chemosphere.2016.10.121

Chowdhury ZZ, Abd Hamid SB, Das R, et al (2013) Preparation of Carbonaceous Adsorbents from Lignocellulosic Biomass and Their Use in Removal of Contaminants from Aqueous Solution. BioResources 8:6523–6555. https://doi.org/10.15376/biores.8.4.6523-6555

519 Co CJU, Quitain AT, Borja JQ, et al (2017) Synthesis and characterization of hybrid
520 composite aerogels from alginic acid and graphene oxide. IOP Conf Ser Mater Sci Eng
521 206:012053. https://doi.org/10.1088/1757-899X/206/1/012053
522 Ersan G, Apul OG, Perreault F, Karanfil T (2017) Adsorption of organic contaminants by
523 graphene nanosheets: A review. Water Res 126:385–398.
524 https://doi.org/10.1016/j.watres.2017.08.010
525 Fei Y, Yong L, Sheng H, Jie M (2016) Journal of Colloid and Interface Science Adsorptive
526 removal of ciprofloxacin by sodium alginate / graphene oxide composite beads from
527 aqueous solution. J Colloid Interface Sci 484:196–204.
528 https://doi.org/10.1016/j.jcis.2016.08.068
529 Feng J, Ding H, Yang G, et al (2017) Preparation of black-pearl reduced graphene oxide–
530 sodium alginate hydrogel microspheres for adsorbing organic pollutants. J Colloid
531 Interface Sci 508:387–395. https://doi.org/10.1016/j.jcis.2017.07.113
532 Fraga TJM, Carvalho MN, Ghislandi MG, Motta Sobrinho MA da (2019) Functionalized
533 Graphene-based materials as innovative adsorbents of organic pollutants: A concise
534 overview. Brazilian J Chem Eng 36:1–31. https://doi.org/10.1590/0104-
535 6632.20190361s20180283
536 Ganesan K, Budtova T, Ratke L, et al (2018) Review on the Production of Polysaccharide
537 Aerogel Particles. Materials (Basel) 11:2144. https://doi.org/10.3390/ma11112144
538 Gao X, Guo C, Hao J, et al (2020) Adsorption of heavy metal ions by sodium alginate based
539 adsorbent-a review and new perspectives. Int J Biol Macromol 164:4423–4434.
540 https://doi.org/10.1016/j.ijbiomac.2020.09.046
541 Grossi A, Laia S De, Souza E De, et al (2014) a Study of Sodium Alginate and Calcium
542 Chloride Interaction. Brazilian Congr Eng Mater Sci 7341–7348
543 Guo W, Hu W, Pan J, et al (2011) Selective adsorption and separation of BPA from aqueous

544 solution using novel molecularly imprinted polymers based on kaolinite/Fe3O4
545 composites. Chem Eng J 171:603–611. https://doi.org/10.1016/j.cej.2011.04.036
546 He J, Ni F, Cui A, et al (2020) New insight into adsorption and co-adsorption of arsenic and
547 tetracycline using a Y-immobilized graphene oxide-alginate hydrogel: Adsorption
548 behaviours and mechanisms. Sci Total Environ 701:134363.
549 https://doi.org/10.1016/j.scitotenv.2019.134363
550 Huang Y, Wang Z (2018) Preparation of composite aerogels based on sodium alginate, and
551 its application in removal of Pb2+and Cu2+from water. Int J Biol Macromol 107:741–
552 747. https://doi.org/10.1016/j.ijbiomac.2017.09.057
553 Hwang N, Barron AR BET Surface Area Analysis of Nanoparticles. 1–11
554 Ionita M, Pandele MA, Iovu H (2013) Sodium alginate / graphene oxide composite films with
555 enhanced thermal and mechanical properties. 94:339–344
556 Jiao C, Xiong J, Tao J, et al (2016) International Journal of Biological Macromolecules
557 Sodium alginate / graphene oxide aerogel with enhanced strength – toughness and its
558 heavy metal adsorption study. Int J Biol Macromol 83:133–141.
559 https://doi.org/10.1016/j.ijbiomac.2015.11.061
560 Junaidi NFD, Othman NH, Shahruddin MZ, et al (2020) Fabrication and characterization of
561 graphene oxide–polyethersulfone (GO–PES) composite flat sheet and hollow fiber
562 membranes for oil–water separation. J Chem Technol Biotechnol 95:1308–1320.
563 https://doi.org/10.1002/jctb.6366
564 Lazim ZM, Salmiati, Hadibarata T, et al (2020) Bisphenol A Removal by Adsorption Using
565 Waste Biomass: Isotherm and Kinetic Studies. Biointerface Res Appl Chem 11:8467–
566 8481. https://doi.org/10.33263/BRIAC111.84678481
567 Li Y, Du Q, Liu T, et al (2013) Methylene blue adsorption on graphene oxide/calcium
568 alginate composites. Carbohydr Polym 95:501–507.

https://doi.org/10.1016/j.carbpol.2013.01.094

Li Y, Jin F, Wang C, et al (2015) Modification of bentonite with cationic surfactant for the enhanced retention of bisphenol A from landfill leachate. Environ Sci Pollut Res 22:8618–8628. https://doi.org/10.1007/s11356-014-4068-0

Liu F, Dai Y, Zhang S, et al (2018) Modification and application of mesoporous carbon adsorbent for removal of endocrine disruptor bisphenol A in aqueous solutions. J Mater Sci 53:2337–2350. https://doi.org/10.1007/s10853-017-1705-2

Liu X, Hu Y, Huang J, Wei C (2016) Detailed characteristics of adsorption of bisphenol A by highly hydrophobic MCM-41 mesoporous molecular sieves. Res Chem Intermed 42:7169–7183. https://doi.org/10.1007/s11164-016-2526-7

Martín-Lara MA, Calero M, Ronda A, et al (2020) Adsorptive Behavior of an Activated Carbon for Bisphenol A Removal in Single and Binary (Bisphenol A—Heavy Metal) Solutions. Water 12:2150. https://doi.org/10.3390/w12082150

Martínez-Gómez F, Guerrero J, Matsuhiro B, Pavez J (2018) Characterization of poly-d-mannuronate and poly-l-guluronate block fractions from sodium alginate and preparation of hydrogels with poly(vinylalcohol). Int J Biol Macromol 111:935–946. https://doi.org/10.1016/j.ijbiomac.2018.01.097

Nie L, Liu C, Wang J, et al (2015) Effects of surface functionalized graphene oxide on the behavior of sodium alginate. Carbohydr Polym 117:616–623. https://doi.org/10.1016/j.carbpol.2014.08.104

Ohore OE, Songhe Z (2019) Endocrine disrupting effects of bisphenol A exposure and recent advances on its removal by water treatment systems. A review. Sci African 5:e00135. https://doi.org/10.1016/j.sciaf.2019.e00135

Othman NH, Alias NH, Shahruddin MZ, et al (2017) Supported graphene oxide hollow fibre membrane for oily wastewater treatment. In: AIP Conference Proceedings

Othman NH, Alias NH, Shahruddin MZ, et al (2018) Adsorption kinetics of methylene blue dyes onto magnetic graphene oxide. J Environ Chem Eng. https://doi.org/10.1016/j.jece.2018.04.024

Park Y, Sun Z, Ayoko GA, Frost RL (2014) Bisphenol A sorption by organo-montmorillonite: Implications for the removal of organic contaminants from water. Chemosphere 107:249–256. https://doi.org/10.1016/j.chemosphere.2013.12.050

Pathania D, Sharma S, Singh P (2017) Removal of methylene blue by adsorption onto activated carbon developed from Ficus carica bast. Arab J Chem 10:S1445–S1451. https://doi.org/10.1016/j.arabjc.2013.04.021

Peng W, Li H, Liu Y, Song S (2017) A review on heavy metal ions adsorption from water by graphene oxide and its composites. J Mol Liq 230:496–504. https://doi.org/10.1016/j.molliq.2017.01.064

Petrie B, Lopardo L, Proctor K, et al (2019) Assessment of bisphenol-A in the urban water cycle. Sci Total Environ 650:900–907. https://doi.org/10.1016/j.scitotenv.2018.09.011

Platero E, Emilia M, Ricardo P, Lea A (2017a) Journal of Colloid and Interface Science Graphene oxide / alginate beads as adsorbents : Influence of the load and the drying method on their physicochemical-mechanical properties and adsorptive performance. J Colloid Interface Sci 491:1–12. https://doi.org/10.1016/j.jcis.2016.12.014

Platero E, Fernandez ME, Bonelli PR, Cukierman AL (2017b) Graphene oxide/alginate beads as adsorbents: Influence of the load and the drying method on their physicochemical-mechanical properties and adsorptive performance. J Colloid Interface Sci 491:1–12. https://doi.org/10.1016/j.jcis.2016.12.014

Seachrist DD, Bonk KW, Ho SM, et al (2016) A review of the carcinogenic potential of bisphenol A. Reprod Toxicol 59:167–182. https://doi.org/10.1016/j.reprotox.2015.09.006

619 Sophia A. C, Lima EC (2018) Removal of emerging contaminants from the environment by
620 adsorption. Ecotoxicol Environ Saf 150:1–17.
621 https://doi.org/10.1016/j.ecoenv.2017.12.026
622 Sun L, Fugetsu B (2014) Graphene oxide captured for green use: Influence on the structures
623 of calcium alginate and macroporous alginic beads and their application to aqueous
624 removal of acridine orange. Chem Eng J 240:565–573.
625 https://doi.org/10.1016/j.cej.2013.10.083
626 Tian X, Zhu H, Meng X, et al (2020) Amphiphilic Calcium Alginate Carbon Aerogels:
627 Broad-Spectrum Adsorbents for Ionic and Solvent Dyes with Multiple Functions for
628 Decolorized Oil–Water Separation. ACS Sustain Chem Eng 8:12755–12767.
629 https://doi.org/10.1021/acssuschemeng.0c00129
630 Wang C, Yang S, Ma Q, et al (2017) Preparation of carbon nanotubes / graphene hybrid
631 aerogel and its application for the adsorption of organic compounds. Carbon N Y
632 118:765–771. https://doi.org/10.1016/j.carbon.2017.04.001
633 Wang J, Zhang M (2020) Adsorption Characteristics and Mechanism of Bisphenol A by
634 Magnetic Biochar. Int J Environ Res Public Health 17:1075.
635 https://doi.org/10.3390/ijerph17031075
636 Wu Y, Qi H, Shi C, et al (2017) Preparation and adsorption behaviors of sodium alginate-
637 based adsorbent-immobilized β-cyclodextrin and graphene oxide. RSC Adv 7:31549–
638 31557. https://doi.org/10.1039/c7ra02313h
639 Xu J, Wang L, Zhu Y (2012) Decontamination of Bisphenol A from Aqueous Solution by
640 Graphene Adsorption. Langmuir 28:8418–8425. https://doi.org/10.1021/la301476p
641 Yang CZ, Yaniger SI, Jordan VC, et al (2011) Most plastic products release estrogenic
642 chemicals: A potential health problem that can be solved. Environ Health Perspect
643 119:989–996. https://doi.org/10.1289/ehp.1003220

644 Yang X, Zhou T, Ren B, et al (2018) Removal of Mn (II) by Sodium Alginate/Graphene
645 Oxide Composite Double-Network Hydrogel Beads from Aqueous Solutions. Sci Rep
646 8:10717. https://doi.org/10.1038/s41598-018-29133-y
647 Zhao P, Yu F, Wang R, et al (2018) Chemosphere Sodium alginate / graphene oxide hydrogel
648 beads as permeable reactive barrier material for the remediation of cipro fl oxacin-
649 contaminated groundwater. Chemosphere 200:612–620.
650 https://doi.org/10.1016/j.chemosphere.2018.02.157
651 Zhou F, Feng X, Yu J, Jiang X (2018) High performance of 3D porous
652 graphene/lignin/sodium alginate composite for adsorption of Cd(II) and Pb(II). Environ
653 Sci Pollut Res 25:15651–15661. https://doi.org/10.1007/s11356-018-1733-8
654

Figures

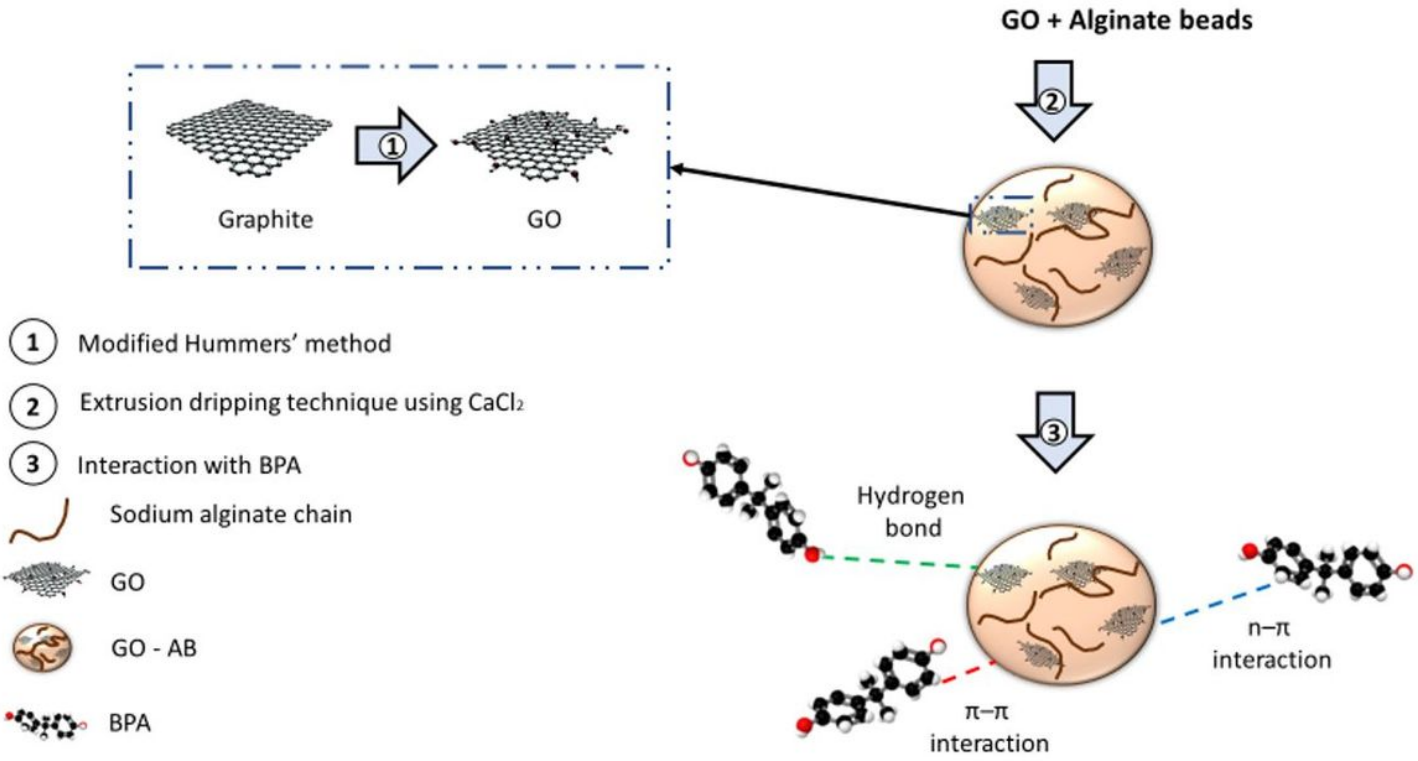

Figure 1

The schematic diagram of interaction between GO and alginate forming GO-alginate beads (GO-AB)

Figure 2

Photograph of extruded aerogel beads in CaCl2 solution

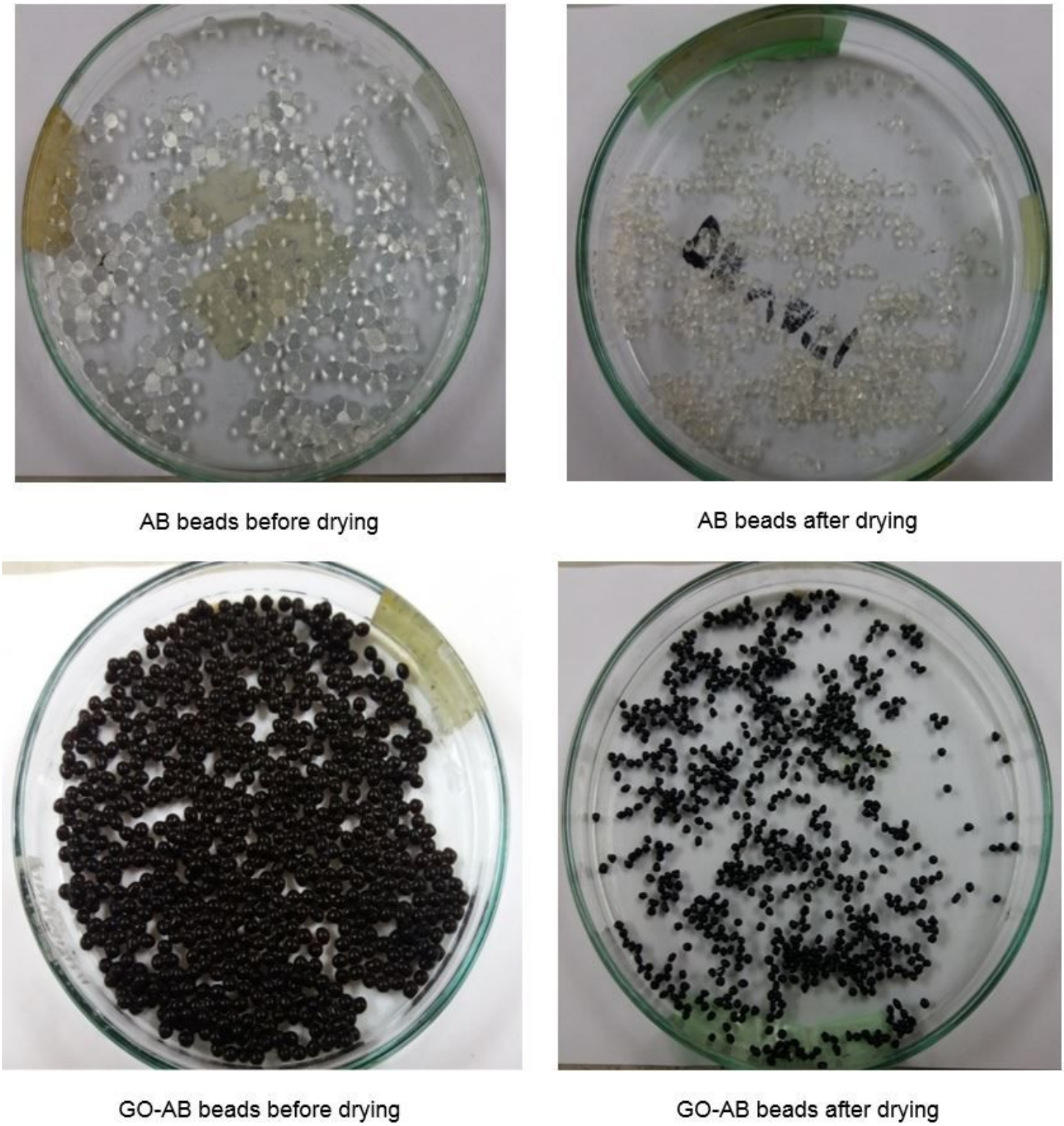

Figure 3

Photograph of alginate bead (AB) and graphene oxide-alginate beads (GO-AB) prepared in this work, before and after drying.

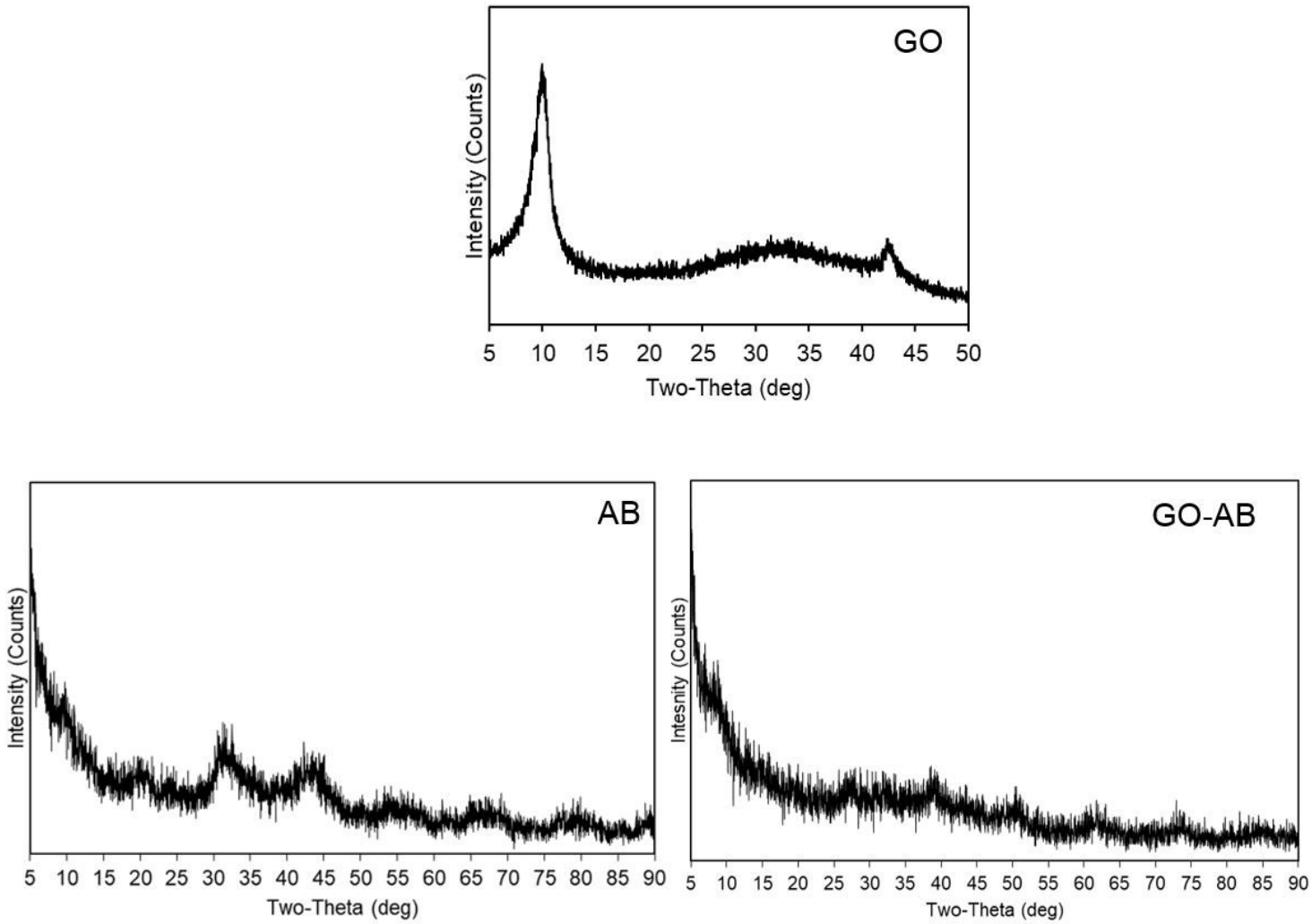

Figure 4

XRD spectra of GO, AB, and GO-AB

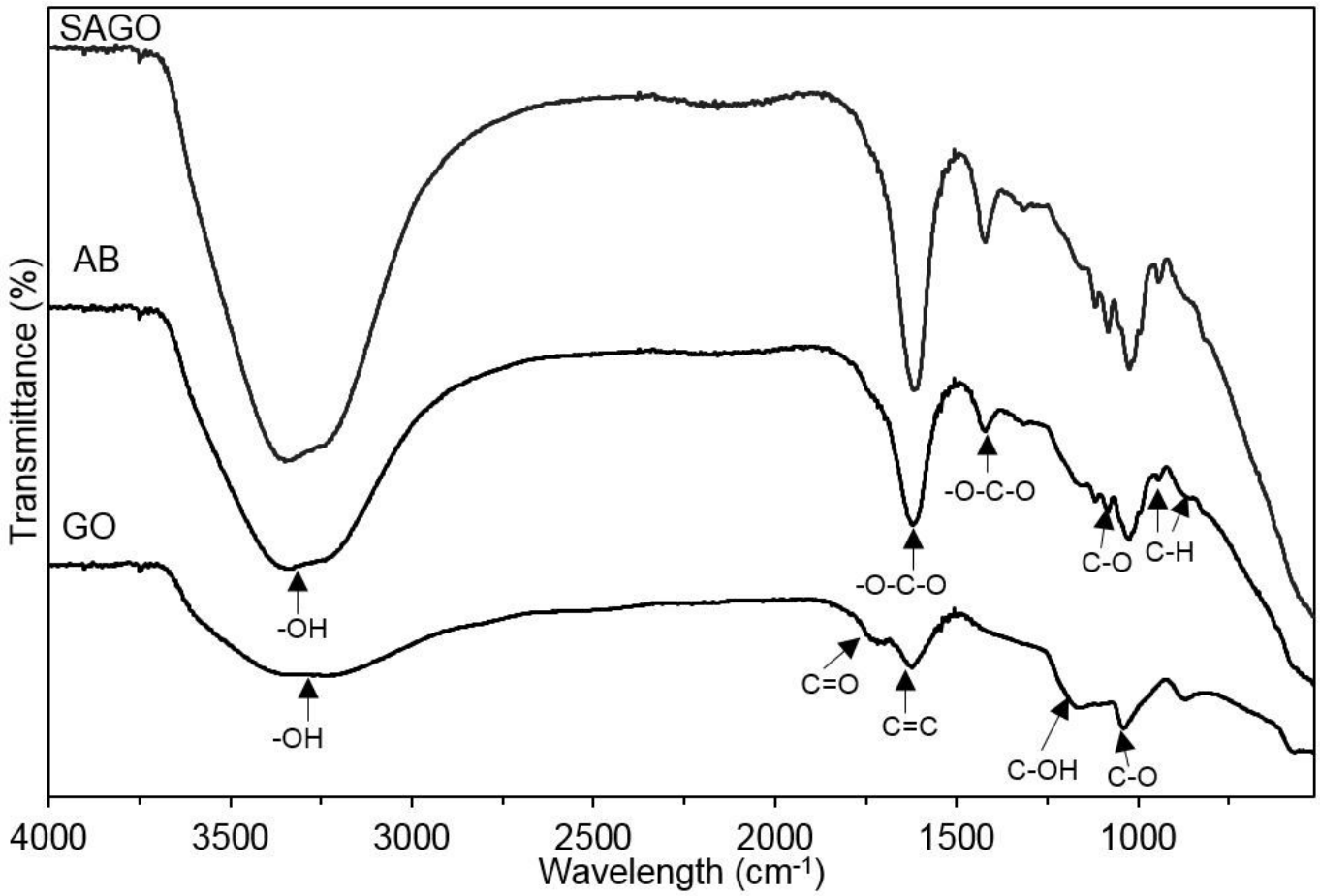

Figure 5

FTIR spectra of GO, AB, and GO-AB aerogels.

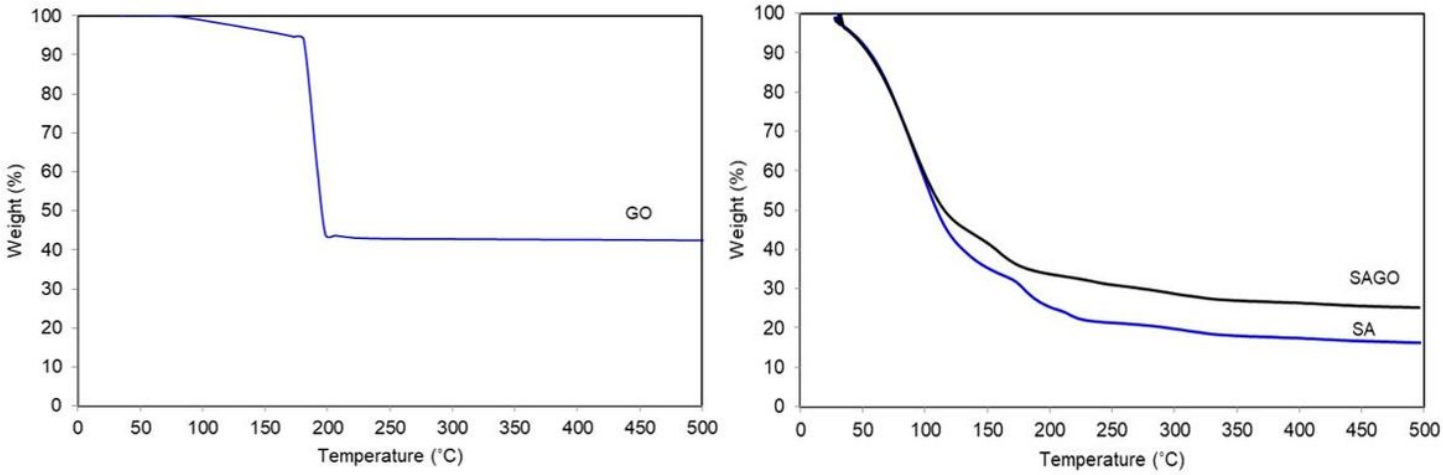

Figure 6

TGA of GO, AB, and GO-AB

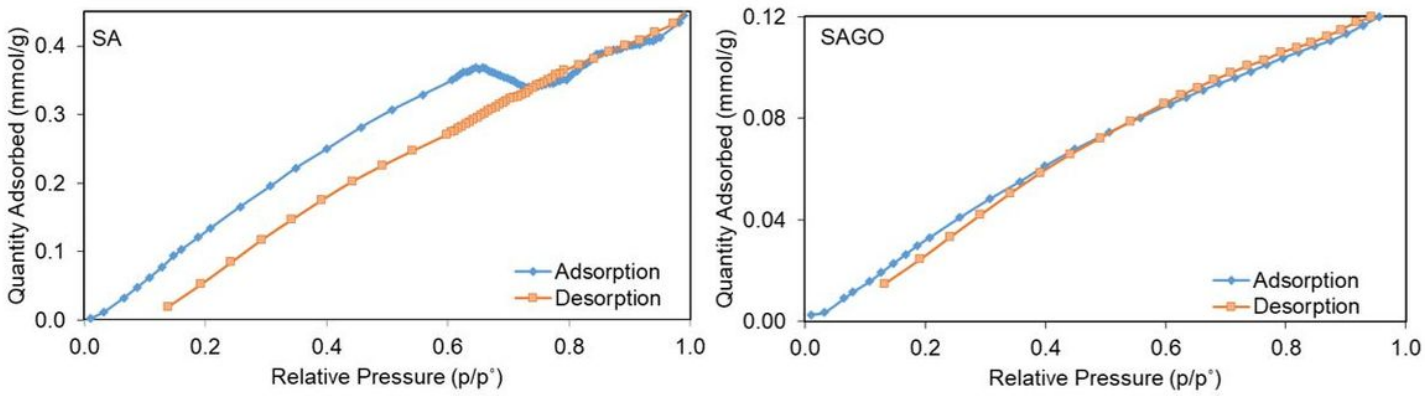

Figure 7

Nitrogen adsorption –desorption measurement of AB and GO-AB adsorbents

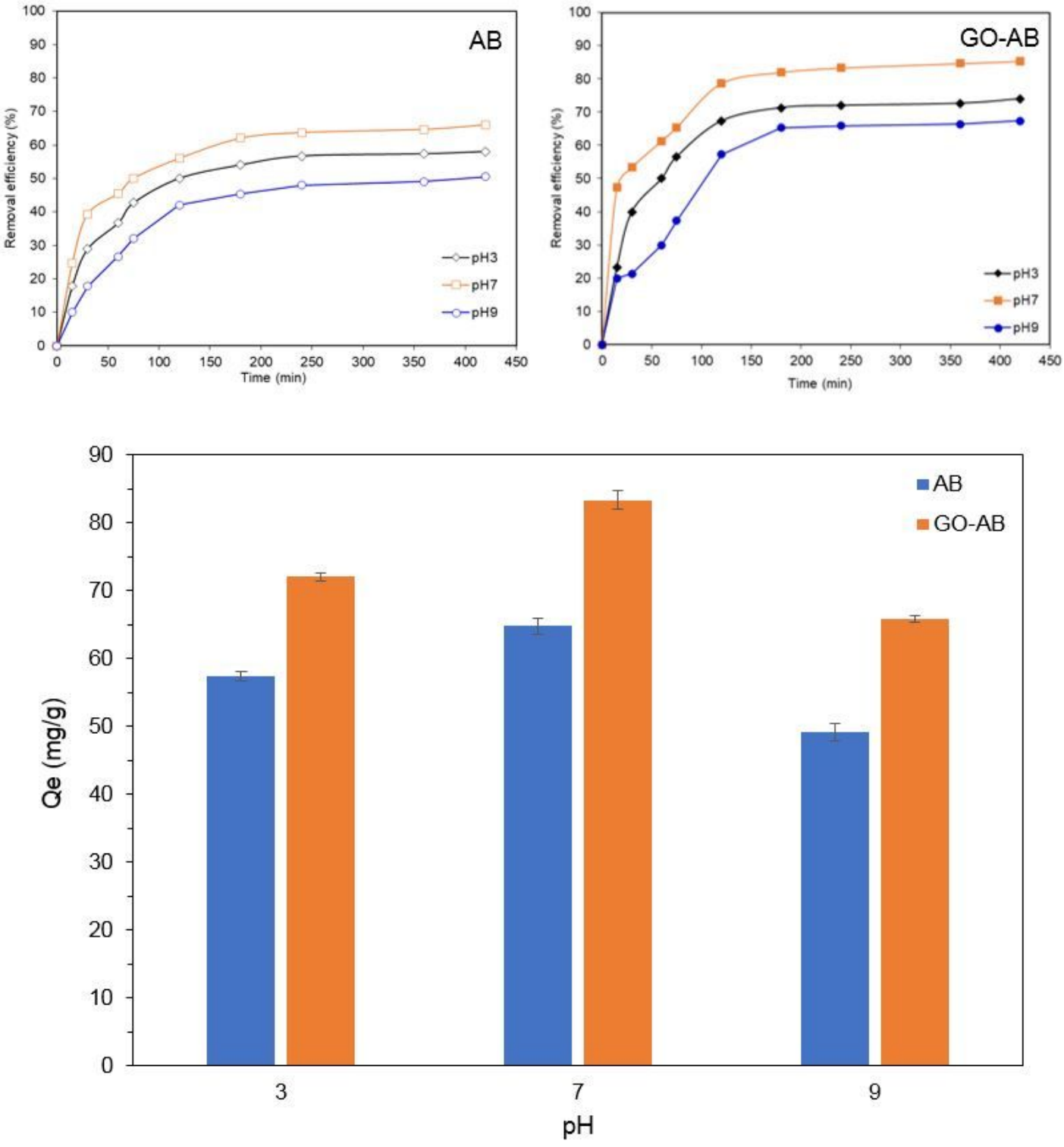

Figure 8

Removal efficiencies and adsorption capacities of AB and GO-AB towards BPA at pH values of 3, 7, and 9 (Mass of adsorbent and initial concentration of BPA were fixed at 0.5 g·L-1 and 50 mg·L-1, respectively)

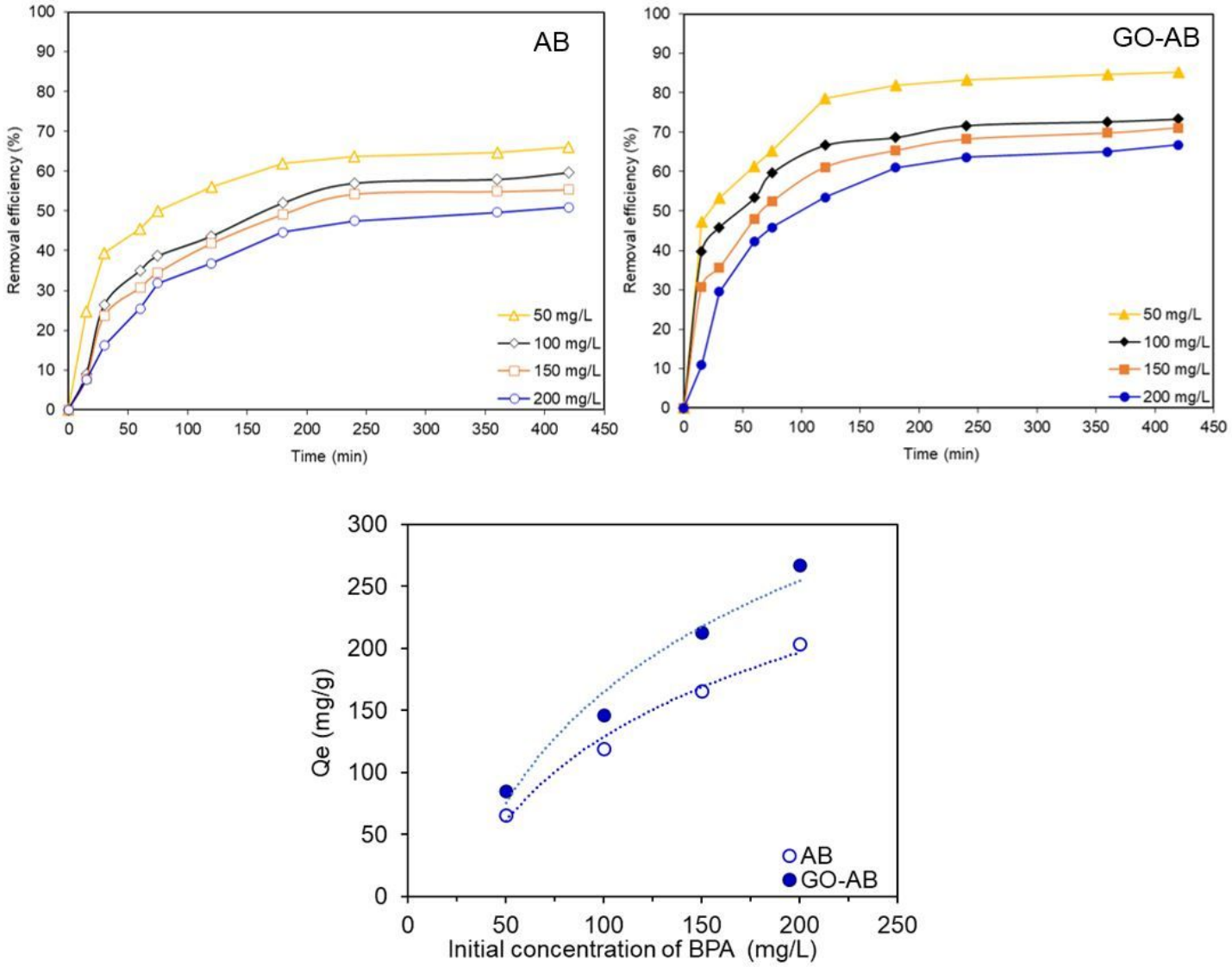

Figure 9

Effects of BPA initial concentrations (C0=50, 100, 150, and 200 50 mg·L-1) on adsorbent performances in term of removal efficiency and adsorption capacity (Mass of adsorbent and pH were set at 0.5 g·L-1 and 7, respectively.

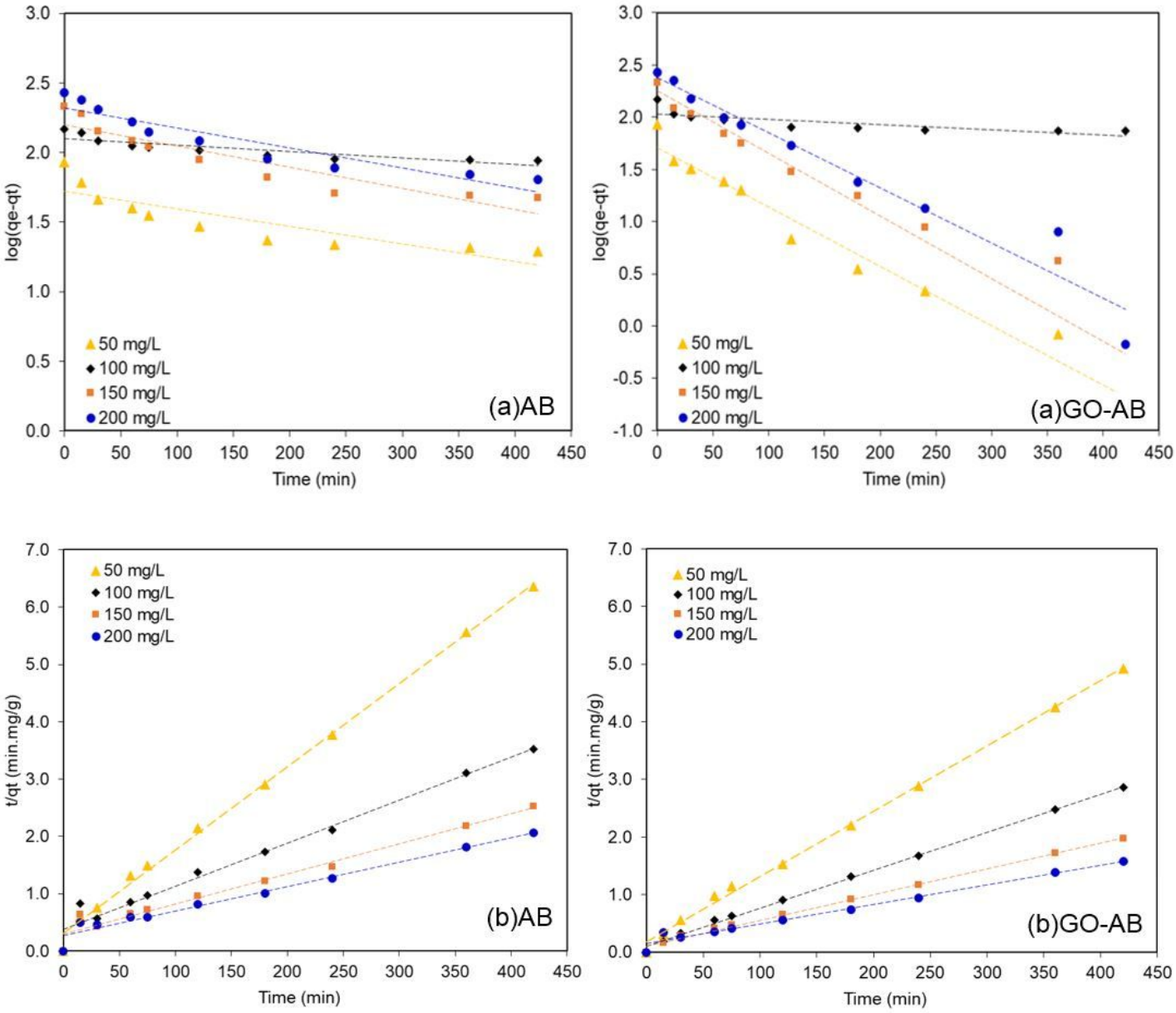

Figure 10

Experimental kinetics data (a) pseudo first order (PFO) and (b) pseudo second order (PSO) for the adsorption of BPA by AB and GO-AB. The dotted lines show the predicted values of the best-fitted model.

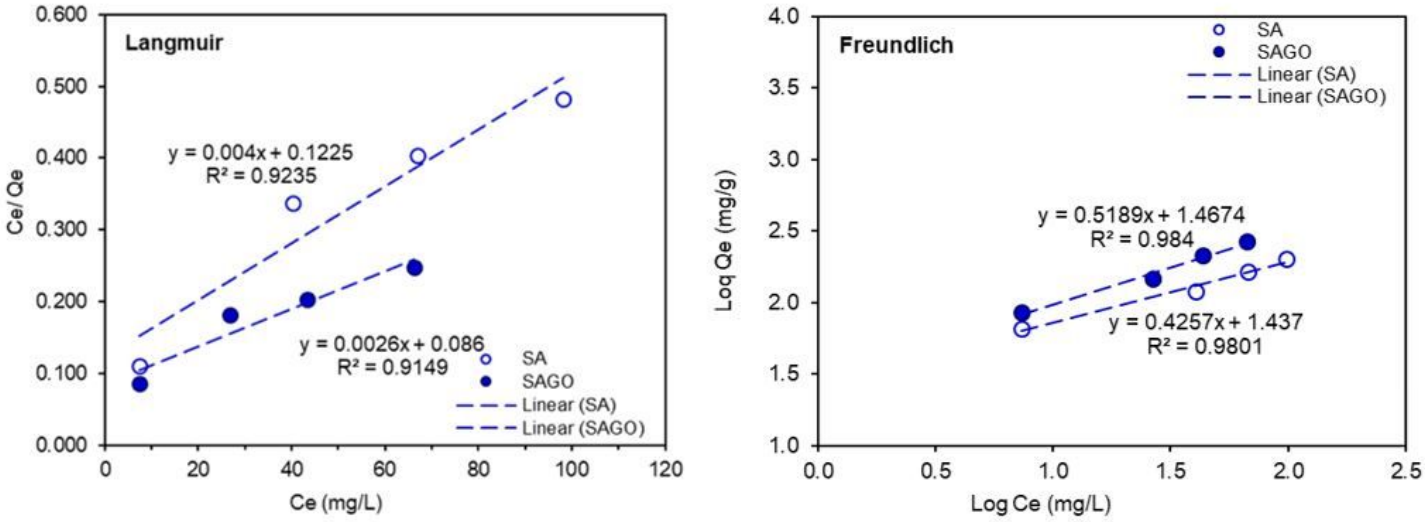

Figure 11

Langmuir and Freudlich isotherm plots for AB and GO-AB